Cell type-specific role of CBX2 and its disordered region in spermatogenesis

Jongmin J. Kim,[1,2] Emma R. Steinson,[1] Mei Sheng Lau,[3] Dirk G. de Rooij,[4] David C. Page,[5,6,7] and Robert E. Kingston[1,2]

[1]Department of Molecular Biology, MGH Research Institute, Massachusetts General Hospital, Boston, Massachusetts 02114, USA; [2]Department of Genetics, Harvard Medical School, Boston, Massachusetts 02115, USA; [3]Institute of Molecular and Cell Biology (IMCB), Agency for Science, Technology, and Research (A*STAR), Proteos, Singapore 138673, Republic of Singapore; [4]Reproductive Biology Group, Division of Developmental Biology, Department of Biology, Faculty of Science, Utrecht University, Utrecht 3584 CH, the Netherlands; [5]Whitehead Institute, Cambridge, Massachusetts 02142, USA; [6]Howard Hughes Medical Institute, Whitehead Institute, Cambridge, Massachusetts 02142, USA; [7]Department of Biology, Massachusetts Institute of Technology, Cambridge, Massachusetts 02139, USA

Polycomb group (PcG) proteins maintain the repressed state of lineage-inappropriate genes and are therefore essential for embryonic development and adult tissue homeostasis. One critical function of PcG complexes is modulating chromatin structure. Canonical Polycomb repressive complex 1 (cPRC1), particularly its component CBX2, can compact chromatin and phase-separate in vitro. These activities are hypothesized to be critical for forming a repressed physical environment in cells. While much has been learned by studying these PcG activities in cell culture models, it is largely unexplored how cPRC1 regulates adult stem cells and their subsequent differentiation in living animals. Here, we show in vivo evidence of a critical nonenzymatic repressive function of cPRC1 component CBX2 in the male germline. CBX2 is up-regulated as spermatogonial stem cells differentiate and is required to repress genes that were active in stem cells. CBX2 forms condensates (similar to previously described Polycomb bodies) that colocalize with target genes bound by CBX2 in differentiating spermatogonia. Single-cell analyses of mosaic *Cbx2* mutant testes show that CBX2 is specifically required to produce differentiating A1 spermatogonia. Furthermore, the region of CBX2 responsible for compaction and phase separation is needed for the long-term maintenance of male germ cells in the animal. These results emphasize that the regulation of chromatin structure by CBX2 at a specific stage of spermatogenesis is critical, which distinguishes this from a mechanism that is reliant on histone modification.

[*Keywords*: Polycomb body; Polycomb repressive complex 1; adult stem cell; chromatin compaction; phase separation; spermatogonia]

Supplemental material is available for this article.

Received December 30, 2022; revised version accepted July 28, 2023.

Polycomb group (PcG) proteins are critical for the stable inheritance of the repressed state of gene expression in development. By regulating chromatin structure and modifications of target genes, PcG proteins create a heritable repressed state over multiple divisions of cells that lack the signal that generated the repressed state (Blackledge and Klose 2021). Adult stem and progenitor cells require PcG proteins for both their maintenance and differentiation (Flora et al. 2021). Many tissues in adult animals, such as blood and skin, are constantly replenished by rare adult stem cells. These cells are capable of self-renewal and can make all differentiated cell types in the lineage. Genetic ablation of certain core PcG proteins, such as *Ring1a/b* or *Eed*, results in failure of maintenance of blood (Piunti et al. 2014; Xie et al. 2014), skin (Dauber et al. 2016), intestine (Chiacchiera et al. 2016; Koppens et al. 2016), and male germline lineages (Mu et al. 2014; Maezawa et al. 2017). Some PcG proteins repress premature senescence to facilitate adult stem cell maintenance (Lessard and Sauvageau 2003; Molofsky et al. 2003; Park et al. 2003). As cancers often originate from misregulated adult stem and progenitor cells, mutations in PcG genes are associated with different types of human cancers (Parreno et al. 2022).

The cellular mechanisms of PcG proteins' role in tissue homeostasis and cancer are poorly understood. This is partly because the complex behavior of adult stem and progenitor cells in their native tissue environment cannot

Corresponding author: kingston@molbio.mgh.harvard.edu
Article published online ahead of print. Article and publication date are online at http://www.genesdev.org/cgi/doi/10.1101/gad.350393.122. Freely available online through the *Genes & Development* Open Access option.

be easily modeled with the cell culture systems. Adult stem and progenitor cells are heterogeneous with different rates of proliferation and self-renewal capacity (Li and Clevers 2010). Understanding potentially distinct functions of PcG proteins in different cellular contexts in an animal is critical for delineating the physiological effects that result from specific PcG dysfunction.

To achieve heritable gene silencing, PcG proteins covalently modify histones and modulate chromatin structure. PcG proteins form three major types of stable multiprotein complexes in the nucleus. One such complex, Polycomb repressive complex 2 (PRC2), catalyzes monomethylation, dimethylation, and trimethylation of the Lys27 residue of H3 (H3K27me1/2/3) (Fig. 1A; Cao et al. 2002; Czermin et al. 2002; Kuzmichev et al. 2002; Müller et al. 2002). H3K27me3 is not sufficient for gene silencing. Canonical PRC1 (cPRC1), which is recruited by its interaction with H3K27me3, is also needed for the maintenance of gene repression by modulating chromatin structure. cPRC1, the focus of this study, is composed of RING1B (or its paralog, RING1A), PCGF2 (or its paralog, PCGF4), CBX2 (or its paralogs, CBX4/6/7/8), and PHC2 (or its paralogs, PHC1/3) (Fig. 1A; Shao et al. 1999; Levine et al. 2002; Gao et al. 2012). cPRC1 can compact polynucleosome arrays (Francis et al. 2004; Grau et al. 2011), phase-separate in vitro (Plys et al. 2019; Tatavosian et al. 2019; Seif et al. 2020), and mediate long-range interactions between distant PcG target loci (Isono et al. 2013; Kundu

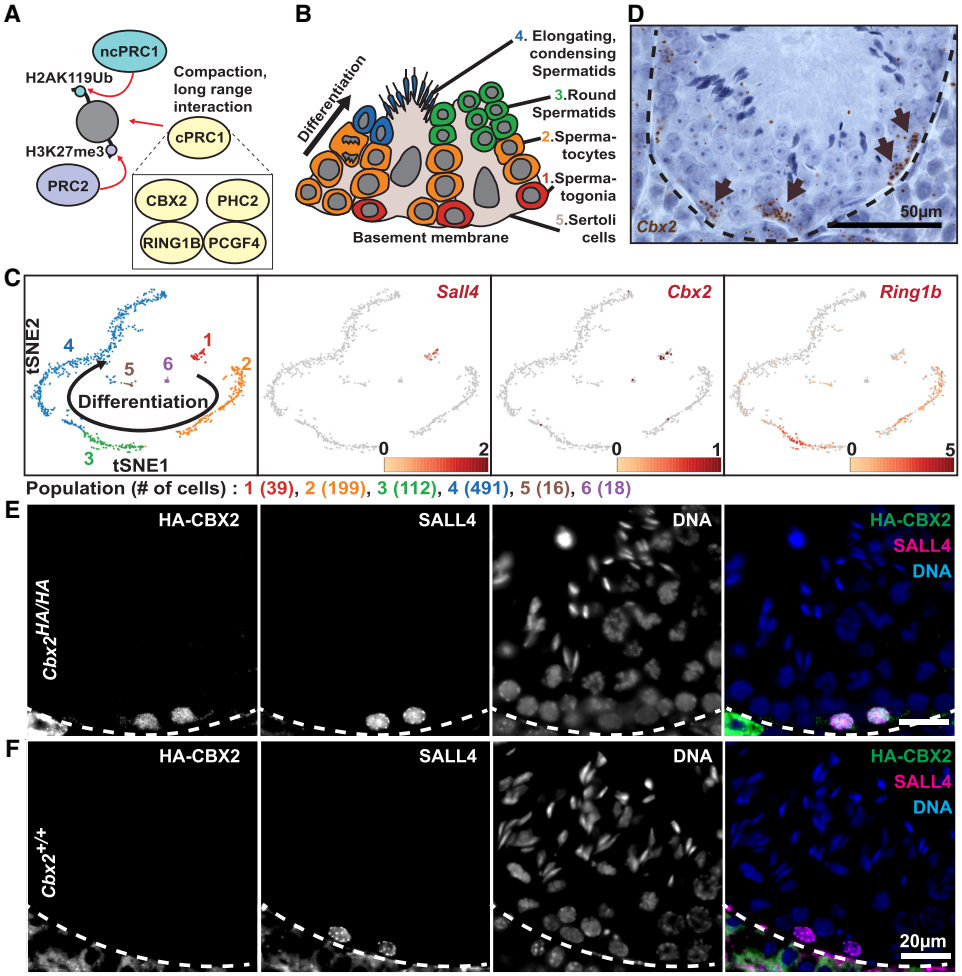

Figure 1. CBX2 is expressed in spermatogonia. (*A*) Schematic representing PcG complexes' functions on chromatin. Individual components of cPRC1 are depicted in the rectangle. (*B*) Schematic of cellular organization in the seminiferous tubule. Note that to show all the major steps in spermatogenesis in one picture, this schematic does not reflect stereotypical cellular organizations based on different tubule stages. (*C*) t-SNE representation of scRNA-seq results from adult testes. The arrow indicates the direction of germ cell differentiation based on known marker gene expression. Numbers 1–5 correspond to different cell types depicted in *B*, and 6 represents Leydig cells. Normalized expression levels of *Sall4*, *Cbx2*, and *Ring1b* are represented in red. Color bars represent expression levels. (*D*) RNA in situ hybridization of *Cbx2* using branched signal amplification, with each brown dot representing a single *Cbx2* RNA transcript. The black dotted line represents the basement membrane of a seminiferous tubule. Brown arrows indicate $Cbx2^{+}$ cells residing at the basement membrane. (*E*,*F*) Coimmunofluorescence staining of testis sections of $Cbx2^{HA/HA}$ (*E*) and $Cbx2^{+/+}$ (*F*) (negative control) animals with HA and SALL4 antibodies. Dotted lines represent the basement membrane. Images are a part of the stage XII tubules.

et al. 2017). These activities contribute to the formation of membraneless nuclear structures called Polycomb bodies (Saurin et al. 1998), which are proposed to be critical for the memory of gene repression (Bantignies et al. 2011; Isono et al. 2013). Mutations disrupting the compaction or oligomerization activities of cPRC1 result in developmental defects (Isono et al. 2013; Lau et al. 2017). These findings suggest that there are critical nonenzymatic roles of cPRC1 in the regulation of chromatin structure and cell fate.

CBX2 is a key component of cPRC1 that is required for its nonenzymatic repressive function. cPRC1 or CBX2 by itself can compact nucleosome arrays, inhibit chromatin remodeling by mSWI/SNF complexes, and phase-separate together with nucleosome arrays in vitro (Grau et al. 2011; Plys et al. 2019; Tatavosian et al. 2019). These activities are dependent on a positively charged and disordered region called the compaction and phase separation (CaPS) region (Supplemental Fig. S1A) of CBX2 (Grau et al. 2011; Jaensch et al. 2021). This region is also required for proper axial development of mice (Lau et al. 2017). Positive charge and disorderedness are conserved features for the compaction activity of other PcG proteins in different species (Beh et al. 2012). Thus, multivalent interactions between PcG proteins, such as CBX2, and nucleosomes through unstructured, charged residues are one important component of PcG activity. CBX2 is essential for many developmental processes. More than 90% of *Cbx2* mutant mice died before weaning, with diverse developmental defects in axial patterning (Core et al. 1997), splenic vasculature (Katoh-Fukui et al. 2005), bone growth (Katoh-Fukui et al. 2019), and sex determination (Katoh-Fukui et al. 1998; Garcia-Moreno et al. 2019). However, in many cases, it remains an open question what specific cell types in development are susceptible to the loss of CBX2.

We set out to test two major questions: whether CBX2 is required at a specific stage of adult stem cell differentiation and whether the compaction and phase separation function of CBX2 is critical for that process. We chose to address these questions using tissue-specific stem cells in living animals. PcG mechanisms have been extensively studied using cultured mouse embryonic stem cells (mESCs). However, mESC chromatin is distinct from most cell types, such that DNA methylation or PRC2 function are dispensable for their survival (Tsumura et al. 2006; Chamberlain et al. 2008). Further investigation in diverse contexts is needed. In particular, molecular mechanisms, such as the role of compaction activity of cPRC1 or formation of Polycomb bodies, have rarely been studied in primary cells in living animals. Thus, we used the male germline to understand the cellular basis and molecular mechanisms governing PcG-mediated adult stem cell regulation.

Germ cells in the testis provide an ideal system to delineate the role of CBX2-cPRC1 function in adult tissue homeostasis. The male germline is a stereotypical adult stem cell lineage, producing sperm essential for continuation of life. A small number of spermatogonial stem cells (SSCs) produce many differentiated sperm throughout the life of the organism. A key regulatory point in spermatogenesis is the irreversible commitment into "differentiating spermatogonia" (de Rooij and Russell 2000). As the daughter cells of SSC divisions become "A-aligned" spermatogonia, they gradually lose their stem cell potential. They down-regulate SSC-enriched genes, such as *Foxc2* (Wei et al. 2018), and reciprocally up-regulate early differentiation genes, such as *Rarg* (*retinoic acid receptor γ*) (Gely-Pernot et al. 2012; Ikami et al. 2015). When stimulated by retinoic acid (RA), some cells from this pool of SSCs and A-aligned spermatogonia irreversibly differentiate to "differentiating spermatogonia" (Fig. 2A; Koubova et al. 2006; Zhou et al. 2008). An important question is how a subset of these cells acquires competence to differentiate by RA stimulation, because the balance between maintenance of SSC pool and differentiation is key to the continued production of sperm (Endo et al. 2015). Given the known role for PcG proteins in cell fate stabilization, we reasoned that CBX2 may play a role in the regulation of spermatogonial differentiation. Other PcG proteins, such as SCML2, SCMH1, RING1B, and EED, were shown to be critical for different steps of spermatogenesis (Takada et al. 2007; Mu et al. 2014; Hasegawa et al. 2015; Maezawa et al. 2017, 2018). None of these proteins were specific for differentiation commitment.

Here, by using inducible as well as CaPS region-specific *Cbx2* mutant mice, we show that CBX2 function is specifically required at the developmental transition from stem cells to committed progenitor cells in spermatogenesis. Single-cell RNA-seq combined with *Cbx2* genotyping using mosaic *Cbx2* mutant animals supported a specific requirement of CBX2 function in the production of committed progenitor cells. The compaction and phase separation region of CBX2 was required for germ cell maintenance in mice. We propose that CBX2 is required for stable repression of the spermatogonial stem cell program to provide competence for irreversible differentiation and that its ability to phase-separate and compact chromatin is essential for these processes.

Results

CBX2 expression coincides with the onset of spermatogonial differentiation

The testis contains spermatogonial stem cells and a continuous stream of differentiating daughter germ cells that eventually become sperm, in addition to somatic supporting cells (Fig. 1B). To identify the cell types that require CBX2 function in spermatogenesis, we profiled the expression of *Cbx2* RNA and protein in the mouse testis. Single-cell RNA-seq of a wild-type testis showed that *Cbx2* expression was enriched in spermatogonia (cluster #1, *Sall4*$^{+}$), while a core PRC1 component, *Ring1b*, was broadly expressed in spermatogonia, spermatocytes, and round spermatids (Fig. 1B,C). Consistent with the single-cell RNA-seq, RNA in situ hybridization showed that *Cbx2* mRNA signal was detected in a small number of cells at the basement membrane, where spermatogonia reside (Fig. 1D). To detect CBX2 protein, we generated a knock-in mouse line in which two tandem HA epitopes

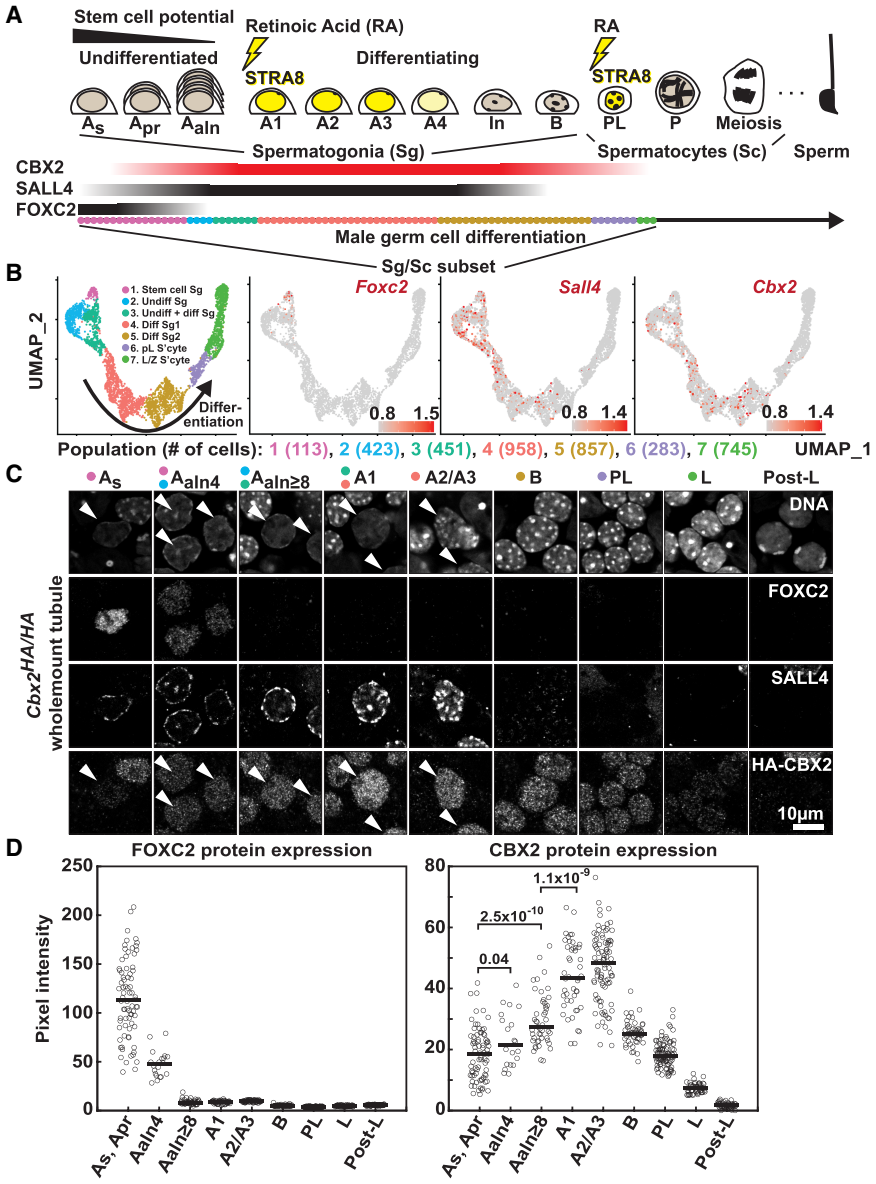

Figure 2. CBX2 is up-regulated as spermatogonial stem cells initiate differentiation. (*A*) Schematic of spermatogonial differentiation in mouse spermatogenesis. (As) A-single, (Apr) A-paired, (Aaln) A-aligned, (In) intermediate, (PL) preleptotene, (P) pachytene. Yellow lightning symbols represent developmental transitions induced by retinoic acid and the ensuing up-regulation of STRA8 (stimulated by retinoic acid 8). Cell types expressing *Foxc2*, *Sall4*, and *Cbx2* are marked by black and red bars. Colored dots at the *bottom* represent corresponding cell types identified in scRNA-seq analyses in *B*. (*B*) UMAP representation of scRNA-seq results from postnatal day 15 (P15) mouse testes (Ernst et al. 2019). P15 UMAP was plotted after obtaining a subset of spermatogonia and early spermatocyte populations from the whole P15 data set. P15 subset cells clustered into seven populations and cell types were assigned according to marker gene expression (marker profiles in Supplemental Fig. S2A). Normalized expression levels of *Foxc2*, *Sall4*, and *Cbx2* are represented in red. (Sg) Spermatogonia, (Undiff) undifferentiated, (diff) differentiating, (pL) preleptotene, (L/Z) leptotene/zygotene. (*C*) Coimmunofluorescence staining of whole-testis tubules of $Cbx2^{HA/HA}$ animals with HA, SALL4, and FOXC2 antibodies. Cellular stages were identified based on the cellular organization along the tubule, the nuclear morphology based on DNA staining, and the protein expression patterns of marker genes, such as FOXC2 and SALL4. (*D*) Quantification of FOXC2 and CBX2 protein expression based on whole-mount tubule stainings. Numbers between groups As, Apr, Aaln4, and Aaln≥8 represent *P*-values calculated by two-tailed *t*-tests.

were inserted in-frame into the N terminus of the endogenous *Cbx2* locus (*HA-Cbx2* mice) (Supplemental Fig. S1A,B and legend). Coimmunostaining of the spermatogonial marker SALL4 and HA-CBX2 in testis sections revealed that CBX2 was expressed in $SALL4^+$ spermatogonia (Fig. 1E,F). All $SALL4^+$ cells expressed CBX2, but CBX2 was also expressed in more differentiated preleptotene spermatocytes that lack SALL4 expression (Supplemental Fig. S1D, stage VII–VIII, arrows) and becomes undetectable in leptotene spermatocytes (Supplemental Fig. S1D, stage IX, arrowheads).

Spermatogonia can be further divided into "undifferentiated" spermatogonia, including spermatogonial stem cells (SSCs), and "differentiating" spermatogonia committed to differentiation (Fig. 2A). As these spermatogonia have distinct properties, such as self-renewal, proliferation rate, and retinoic acid responsiveness, we set out to determine the precise stages of spermatogenesis at which CBX2 is expressed. Since some PRC1 components, such as BMI1 (PCGF4), have been proposed to be a specific marker for SSCs (Komai et al. 2014), we were particularly curious whether CBX2 is expressed in SSCs. To this end, we first used publicly available single-cell RNA-seq data from juvenile mouse testes, which contain a higher proportion of spermatogonia (Ernst et al. 2019). We chose cells classified as spermatogonia and early spermatocytes and reclustered them to generate seven refined clusters of the early cell types (Fig. 2B; Supplemental Fig. S2A). Consistent with our single-cell RNA-seq data from an adult testis, *Cbx2* was expressed in $Sall4^+$ spermatogonia and was down-regulated at spermatocyte stages (Fig. 2B; Supplemental Fig. S2B). Notably, *Cbx2* expression appeared depleted in $Foxc2^+$ spermatogonia known to have high stem cell potential (Fig. 2B; Supplemental Fig. S2B; Wei et al. 2018). Only 4% of $Foxc2^+$ cluster #1 cells contained any *Cbx2* reads, while *Foxc2*-low clusters #2 and #3 each

had 18% and 23% of cells with *Cbx2* reads, respectively (Supplemental Fig. S2B).

Coimmunostaining of CBX2 and FOXC2 also showed lower CBX2 protein expression in undifferentiated FOXC2$^+$ cells than in differentiating spermatogonia. We performed whole-mount tubule staining (Supplemental Fig. S2C) because, unlike in sections, FOXC2$^+$ cells can be categorized into singlets and paired cells (high stem cell potential) to a chain of aligned cells (low stem cell potential). Isolated and paired cells with robust FOXC2 expression showed undetectable to very low CBX2 signal (Fig. 2C,D, As and Apr; Supplemental Fig. S2C, arrow). In contrast, aligned FOXC2$^+$ cells showed higher levels of CBX2 expression than the FOXC2$^+$ As and Apr cells (Fig. 2C,D, Aaln4 and Aaln≥8; Supplemental Fig. S2C, arrowhead). CBX2 expression was further increased in differentiating spermatogonia (Fig. 2C,D, A1 and A2/A3), perdured until preleptotene spermatocytes (Fig. 2C,D, PL), and nearly disappeared as cells matured into the leptotene spermatocyte stage (Fig. 2C,D, L). We conclude that CBX2 is up-regulated as spermatogonia exit from the stem cell state and is robustly expressed in differentiating spermatogonia but is down-regulated as meiosis initiates in leptotene spermatocytes.

CBX2-cPRC1 forms Polycomb bodies in spermatogonia

Chromatin-bound cPRC1 coalesces in membraneless structures called Polycomb bodies (Satijn et al. 1997; Saurin et al. 1998). Although it has been proposed that Polycomb bodies are critical for genome organization and PcG target gene regulation (Bantignies et al. 2011), there is limited evidence to indicate whether Polycomb bodies are formed in primary cells of adult mammals. To ask whether CBX2-cPRC1 forms Polycomb bodies in spermatogonia, we performed coimmunostaining of CBX2 and other cPRC1 proteins using dissociated germ cells. Fine subnuclear structures like Polycomb bodies are better visualized as a dissociated monolayer in single cells than in the intact tissue. We used FACS to purify differentiating spermatogonia with robust CBX2 expression using a cell surface marker, c-KIT, from *Cbx2*$^{HA/+}$ animals (c-KIT expression is specific to differentiating spermatogonia) (Supplemental Fig. S2A; Shinohara et al. 2000). Coimmunostaining of the c-KIT$^+$ spermatogonia with HA and RING1B antibodies showed nonuniform expression of HA-CBX2 in the nucleus, forming ~200-nm (diameter)-sized puncta (Fig. 3A; Supplemental Fig. S3A). In addition, RING1B, which forms cPRC1 with CBX2, also showed a punctate expression pattern, overlapping with CBX2 Polycomb bodies (Fig. 3A, arrows). Not all CBX2 and RING1B puncta overlap, which is in part due to nonspecific staining of antibodies, especially for weak-intensity puncta (Supplemental Fig. S3B). To corroborate the findings using the HA tag, we developed specific polyclonal antibodies against nearly full-length CBX2 protein (Supplemental Fig. S1A,C). Immunostaining of native CBX2 from wild-type c-KIT$^+$ spermatogonia also showed CBX2 forming Polycomb bodies, some of them together with another cPRC1 component, PHC2 (Fig. 3B, arrows). Thus, CBX2-containing cPRC1 is compartmentalized into Polycomb bodies in spermatogonia.

One critical question is whether CBX2 Polycomb bodies represent CBX2-cPRC1 bound to chromatin or, on the contrary, a storage unit sequestered away from target genes, as some reports hypothesized (Saurin et al. 1998). Polycomb bodies were shown to be associated with target DNA, such as a *Hox* locus in fly embryos (Grimaud et al. 2006) and mouse embryonic fibroblasts (MEFs) (Isono et al. 2013), but whether that is true in adult animals has not been addressed. We tested whether CBX2 and RING1B condensates overlap with a classical Polycomb target gene, *HoxD*. A nontarget gene desert region was also probed as a negative control. CUT&RUN experiments using purified spermatogonia (see details in the next section) showed that CBX2 and RING1B were preferentially localized at the *HoxD* locus but not at the gene desert region (Supplemental Fig. S3C). Coimmuno-FISH revealed that both CBX2 and RING1B condensates overlapped with the *HoxD* but not with the gene desert locus (Fig. 3C–F). Not all *HoxD* puncta overlapped CBX2 and RING1B condensates. About one-third of *HoxD* puncta overlapped with distinct CBX2 or RING1B puncta, one-third of *HoxD* puncta overlapped with diffusive CBX2 or RING1B signal, and the remaining one-third of *HoxD* puncta did not overlap with CBX2 or RING1B signal (Supplemental Fig. S3D,E). Importantly, the negative control gene desert puncta never overlapped with CBX2 or RING1B puncta (Fig. 3D,F; Supplemental Fig. S3E). When images centered at *HoxD* or gene desert puncta were averaged, there was corresponding enrichment of CBX2 or RING1B signal at the *HoxD* signal peak, whereas there was no such enrichment for the gene desert locus (Fig. 3G–J). Another *Hox* cluster, *HoxB*, also showed similar CBX2 signal enrichment when *HoxB* puncta signals were averaged (Supplemental Fig. S3F,G), while a negative control protein, SALL4, did not show signal enrichment corresponding to *HoxB* puncta locations. Thus, CBX2 forms Polycomb bodies with other cPRC1 components in spermatogonia, and these Polycomb bodies are associated with target chromatin that harbors silenced genes.

CBX2-cPRC1 binds genes down-regulated as spermatogonial stem cells differentiate

The data presented above are consistent with CBX2-cPRC1 being necessary for the repression of genes that might impede the proper differentiation of spermatogonia. To examine this hypothesis, we identified genes in differentiating spermatogonia that were occupied by CBX2 and cPRC1. We performed CUT&RUN (Skene and Henikoff 2017) in FACS-purified c-KIT$^+$ differentiating spermatogonia (Supplemental Fig. S2A) with antibodies against CBX2, RING1B, PHC2, BMI1 (PCGF4), H3K27me3, and H3K4me3. CBX2 was preferentially enriched at promoters of genes, and its enrichment often spread >10 kb (Fig. 4A,B). We obtained a conservative set of 708 promoters bound by CBX2 based on enrichment of CBX2 using both CBX2 and HA antibodies (Fig. 4B). Notable examples of CBX2 targets identified in this set were

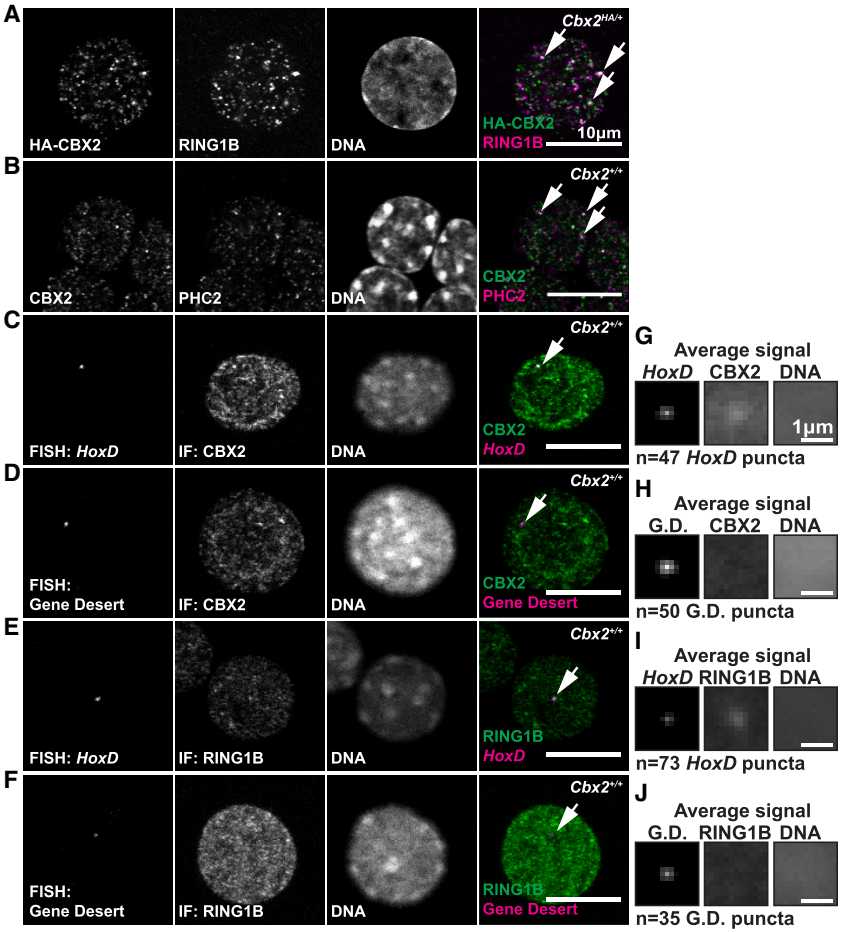

Figure 3. CBX2-cPRC1 forms Polycomb bodies with target DNA. (*A*,*B*) Coimmunostaining of HA-CBX2 and RING1B (*A*) and CBX2 and PHC2 (*B*) using FACS-sorted c-KIT$^+$ spermatogonia from *Cbx2*$^{HA/+}$ (*A*) and wild-type (*B*) mice. (*C*–*F*) Coimmuno-FISH of the *HoxD* locus and CBX2 protein (*C*), the gene desert locus and CBX2 protein (*D*), the *HoxD* locus and RING1B protein (*E*), and the gene desert locus and RING1B protein (*F*) using FACS-sorted c-KIT$^+$ spermatogonia from wild-type mice. A single optical section, which usually contains one allele of *HoxD* or the gene desert locus in the plane, is represented to avoid incidental overlap of puncta at different focal planes. (*G*–*J*) Average signal projection of a 2-μm square centered at *HoxD* or gene desert puncta. Average signal projections of CBX2 or RING1B and DNA at the corresponding locations are also represented.

Foxc2, *Pax7*, and *Gfra1* (Fig. 4A; Supplemental Fig. S4A), key transcription factors and a cell surface receptor specifically expressed in spermatogonial stem cells and their immediate daughter cells (Hofmann et al. 2005; Aloisio et al. 2014; Wei et al. 2018). These genes are normally down-regulated as spermatogonia differentiate. On the contrary, genes robustly expressed in differentiating spermatogonia, such as *Sall4* and *c-Kit*, did not show enrichment of CBX2-cPRC1 (Fig. 4A; Supplemental Fig. S4A). In general, transcripts associated with these 708 promoters collectively had higher expression levels in spermatogonial stem cells and down-regulated as cells differentiated and CBX2 was up-regulated (Fig. 4C; Supplemental Fig. S4B). CUT&RUN analyses of RING1B, BMI1, and PHC2 all showed promoter-centered broad enrichment patterns that mirrored those of CBX2, showing that all four components of cPRC1 colocalized as expected (Fig. 4A,B). H3K27me3, which is bound by CBX2's chromodomain, also had expected overlapping enrichment patterns with CBX2 (Fig. 4A,B). The 708 CBX2/cPRC1/H3K27me3-enriched promoters showed relatively low levels of H3K4me3, with only four out of 708 CBX2 target promoters in the top 5% of 1433 H3K4me3-enriched promoters (Fig. 4B; Supplemental Fig. S4C), consistent with CBX2-cPRC1-bound genes having low transcriptional activity. Furthermore, CBX2 and RING1B showed higher levels of enrichment at 708 target promoters in c-KIT$^+$ differentiating spermatogonia than in THY1$^+$ and ITGa6$^+$ undifferentiated spermatogonia, which include SSCs (Fig. 4D; Supplemental Fig. S4D,E). We conclude that CBX2-PRC1 binds to genes that are normally down-regulated as spermatogonia differentiate.

CBX2 is required for differentiation to CCND2$^+$ A1 spermatogonia

To test the function of CBX2 in spermatogenesis in adult animals, we used an inducible knockout (KO) strategy. We injected tamoxifen into a mouse line that expressed inducible CRE recombinase (*Rosa26-CRE*^{ERT2}) and contained floxed *Cbx2* alleles (Fig. 5A; Supplemental Fig. S5A). We chose an inducible KO strategy because we aimed to assess immediate effects after inducing *Cbx2* deletion to minimize cellular compensation mechanisms. Even though *Rosa26* is a ubiquitous CRE driver, only spermatogonia express CBX2 in adult seminiferous tubules (Fig. 1). Both experimental (CRE$^+$) and control animals received three daily tamoxifen injections. Testes were collected at day 4, and changes in cell type distribution and gene expression were analyzed by single-cell RNA sequencing after FACS purification of c-KIT$^+$ CBX2-expressing spermatogonia (Fig. 5A).

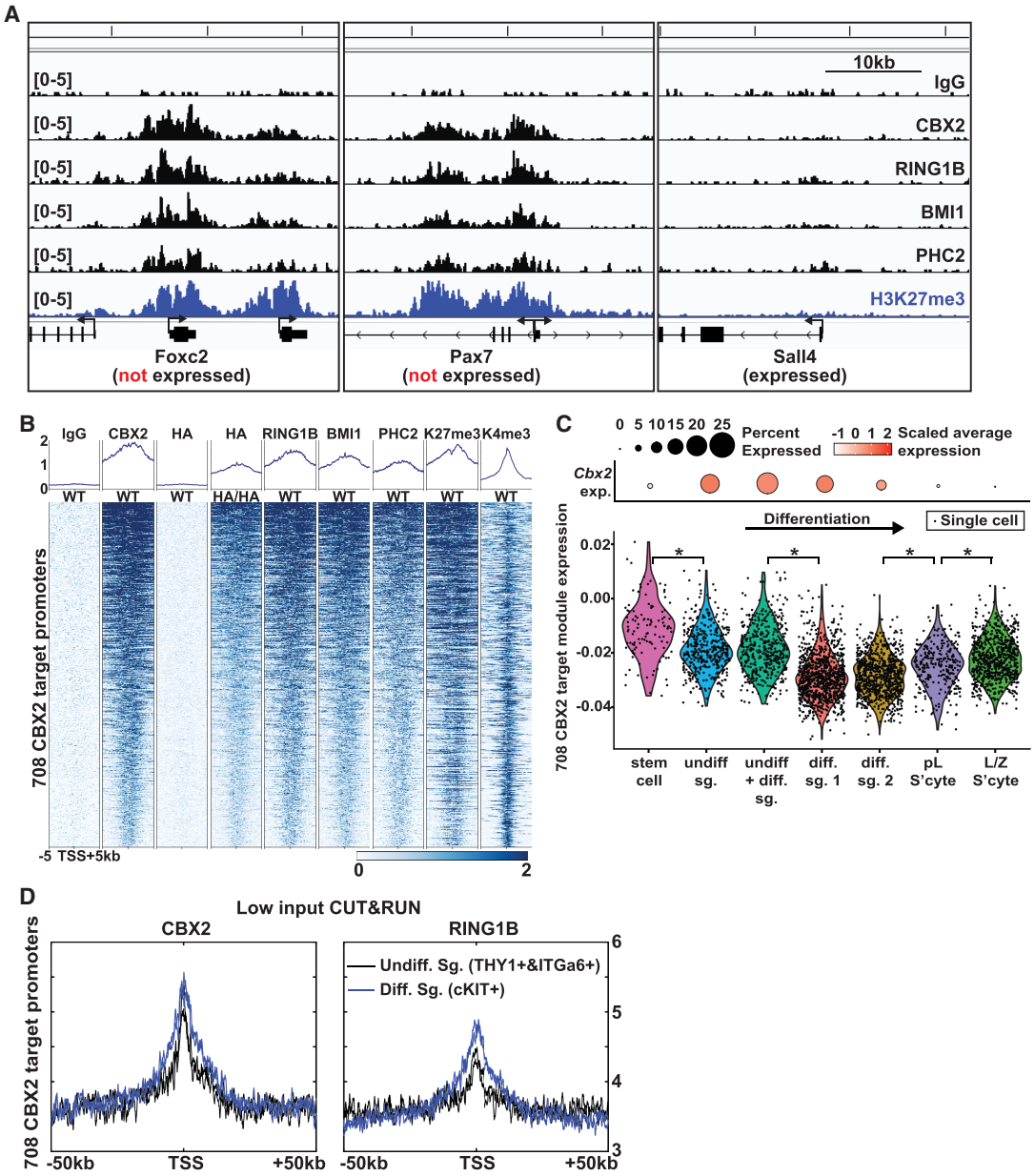

Figure 4. CBX2-cPRC1 binds genes down-regulated as spermatogonial stem cells differentiate. (*A*) Genome browser screenshots of CUT&RUN enrichment of IgG, CBX2, and cPRC1 components (RING1B, BMI1, and PHC2) and H3K27me3 from FACS-sorted c-KIT$^+$ spermatogonia. Enrichment profiles at *Foxc2*, *Pax7*, and *Sall4* genes are shown as representative examples. *Foxc2* and *Pax7* are highly expressed in spermatogonial stem cells and down-regulated in c-KIT$^+$ differentiating spermatogonia. In contrast, *Sall4* is robustly expressed in c-KIT$^+$ spermatogonia. (*B*) Heat maps showing CUT&RUN enrichment of CBX2, cPRC1 components, and associated histone modifications at 708 CBX2 target promoters. (TSS) Transcription start site. (*C*) Average expression levels of the CBX2 target module (genes expressed from 708 CBX2 target promoters) per cell in single-cell clusters represented in Figure 2B. (*) $P < 0.0001$ by one-way ANOVA with post-hoc Tukey's HSD test. *Cbx2* expression depicted in Supplemental Figure S2B is also represented as a comparison. (*D*) Average low-input CUT&RUN enrichment of CBX2 and RING1B at 708 CBX2 target promoters identified in *B*. Profiles for each protein in FACS-sorted undifferentiated (THY1$^+$ and ITGa6$^+$; black lines; two replicates) and differentiating (c-KIT$^+$; blue lines; two replicates) spermatogonia are shown. Signal intensities for the same antibody are trimmed mean of *M*-values (TMMs) normalized using values from all 27,848 promoters ±50 kb centered at TSSs.

Single-cell analyses of sorted c-KIT$^+$ cells identified eight major populations of cells along the differentiation trajectory that encompassed 90% of all profiled cells (Fig. 5B, populations #1–#8); the remaining 10% of cells were classified into three minor populations. As expected, the majority of cells in the eight populations expressed *c-Kit* (Supplemental Fig. S5B). Population #1 was the most undifferentiated, with specific expression of *Ccnd2*,

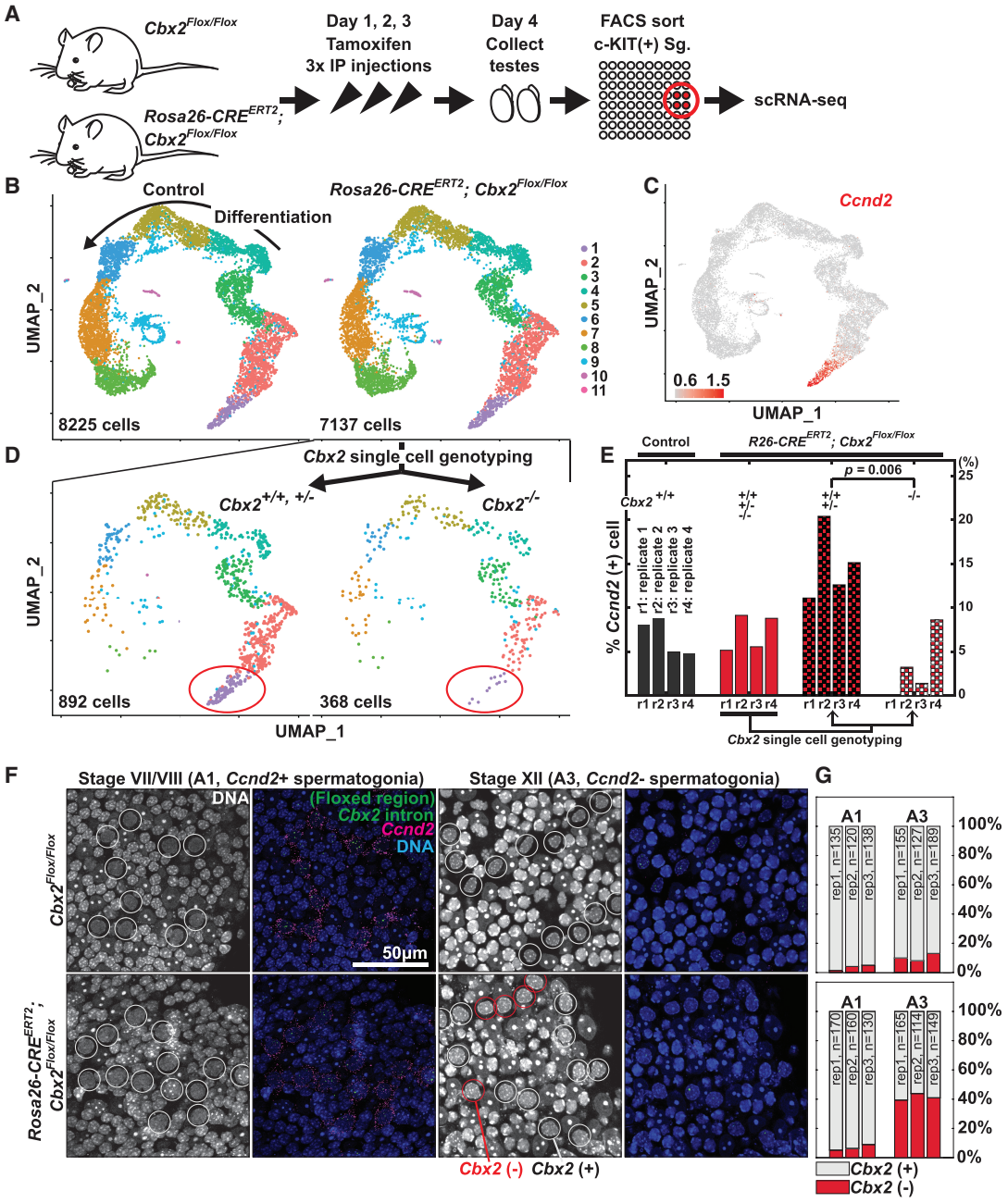

Figure 5. CBX2 is required for differentiation to CCND2$^+$ A1 spermatogonia. (*A*) Schematic representation of experimental steps. (*B*) UMAP representation of a scRNA-seq comparison between FACS-sorted c-KIT$^+$ spermatogonia from control (replicates 1–3: *Cbx2*$^{Flox/Flox}$, tamoxifen-injected; replicate 4: *Rosa26-CRE*^{ERT2}; *Cbx2*$^{Flox/+}$, mock-injected) and *Cbx2*-inducible mutant (replicates 1–4: *Rosa26-CRE*^{ERT2}; *Cbx2*$^{Flox/Flox}$, tamoxifen-injected) animals. Each UMAP is a combined result of four replicates (four animals per condition). (*C*) Normalized expression level of *Ccnd2* is represented on the UMAP of all profiled cells (15,362 cells). (*D*) Separate UMAP representation of *Cbx2*$^{+/+,+/-}$ and *Cbx2*$^{-/-}$ spermatogonia from *Cbx2*-inducible mutant animals after *Cbx2* genotyping using *Cbx2*-specific amplicon sequencing. (*E*) Proportions of *Ccnd2*$^+$ cells (population #1 from *B*) among *Cbx2*-expressing populations (populations #1–#6) in different *Cbx2* genotype categories. Data from four replicates each for control and *Cbx2*-inducible mutant animals are represented. *P*-value was calculated by two-tailed *t*-test. (*F*) Hybridization chain reaction (HCR) RNA-FISH of whole-testis tubules of control (*Cbx2*$^{Flox/Flox}$) and *Cbx2*-inducible mutant (*Rosa26-CRE*^{ERT2}; *Cbx2*$^{Flox/Flox}$) animals with probes against *Ccnd2* (magenta) and the floxed region of *Cbx2* (green) RNA. Stage VII/VIII and XII tubules in which A1 and A3 spermatogonia reside are visualized. Stage VII/VIII was identified by nuclear DNA-staining patterns of characteristic preleptotene spermatocyte morphology and organization and by the presence of aligned condensed spermatid nuclei by scanning different *Z*-planes. Stage XII was identified by the lack of round spermatids and the presence of secondary spermatocytes or spermatocytes in meiotic division. (*G*) Quantification of the proportion of *Cbx2*$^+$ (light gray) and *Cbx2*$^-$ (red) A1 and A3 spermatogonia in *F*. Results from three independent experiments are shown. The number of cells analyzed are listed in the bar plots.

which only marks A1 stage cells among differentiating spermatogonia (Fig. 5C; Supplemental Fig. S2A; Beumer et al. 2000). *Cbx2* was expressed in populations #1–#6, but its expression was diminished in populations #7 and #8, which expressed the second wave of *Stra8* as cells entered the preleptotene stage (Supplemental Fig. S5B). Hence, we focused our subsequent analyses on population #1–#6 cells.

At first glance, scRNA-seq comparison of *Cbx2* mutant (CRE^+) and control animals showed almost identical cellular distributions (Fig. 5B). This was surprising because ablation of PRC1, of which CBX2 is a key component in these cells, was previously shown to cause defects in the male germ cell line (Maezawa et al. 2017). However, the *Cbx2* mutant animals (CRE^+) contained a mix of homozygous wild-type ($Cbx2^{+/+}$), heterozygous ($Cbx2^{+/-}$), and homozygous mutant ($Cbx2^{-/-}$) cells, which we hypothesized obscured any differences between the bulk populations (Fig. 5B). We therefore separated cells obtained from the *Cbx2* mutant animals based on their genotypes, and the genotype-specific analysis revealed a distinct behavior of *Cbx2* homozygous mutant cells (Fig. 5D [red circles], E). We independently sequenced *Cbx2* amplicons generated from the aliquot of cell-barcoded cDNA derived from the samples prepared for single-cell RNA-seq (Materials and Methods; Supplemental Fig. S5A–D and legends). When the cell type distribution of *Cbx2* homozygous mutant cells ($Cbx2^{-/-}$) was compared with the *Cbx2* heterozygous mutant and homozygous wild-type cell distribution within the same testes ($Cbx2^{+/+}$ and $Cbx2^{+/-}$ combined), we noticed a depletion of $Ccnd2^+$ A1 spermatogonia in $Cbx2^{-/-}$ cells (Fig. 5D [red circles], E). Among the CBX2-expressing populations #1–#6, while $Ccnd2^+$ A1 spermatogonia on average occupied 6.7% of cells in four control animals, they occupied only 2.5% of $Cbx2^{-/-}$ cells isolated from the four *Cbx2* mutant (CRE^+) animals (Fig. 5E). In contrast, A1 spermatogonia on average occupied 12.7% of $Cbx2^{+/+,+/-}$ cells isolated from the mutant. The increase in A1 spermatogonia $Cbx2^{+/+\ +/-}$ cells in the mosaic mutant is consistent with the possibility that $Cbx2^{+/+,+/-}$ cells might compensate for the depletion of $Cbx2^{-/-}$ cells within the same testes (Fig. 5E). Note that the last tamoxifen injection was 24 h prior to cell harvesting, which can induce new mutations in later spermatogonia (population #2 and beyond) that had already passed the A1 stage. Only ~10%~20% of the total cells contained sufficient *Cbx2* reads to be confidently genotyped, which may have contributed to the variability of A1 spermatogonia proportion between replicates for genotyped cells. However, all replicates showed consistent trends of specific depletion of $Cbx2^{-/-}$ A1 spermatogonia. In addition, gene expression comparison between $Cbx2^{+/+,+/-}$ and $Cbx2^{-/-}$ spermatogonia (populations #1–#6 combined) identified *Stra8* and *Ccnd2* as the top two down-regulated genes in $Cbx2^{-/-}$ spermatogonia (Supplemental Fig. S5E). *Stra8* (*stimulated by retinoic acid gene 8*) is a gene up-regulated in A1 spermatogonia by retinoic acid stimulation (Fig. 2A; Supplemental Fig. S2A). Lower *Stra8* and *Ccnd2* levels in this population are consistent with the depletion of A1 spermatogonia in $Cbx2^{-/-}$ cells. Based on this single-cell *Cbx2* genotyping of mosaic mutant testis, we conclude that CBX2 plays a key role in the production of A1 spermatogonia.

We confirmed the depletion of $CCND2^+$ A1 spermatogonia by independent RNA-FISH and immunostaining experiments on whole-mount tubules. We generated FISH probes against the deleted region (2920 bp; 94% intronic) to detect *Cbx2* pre-mRNA (Supplemental Fig. S5A, red lines). *Cbx2* RNA-FISH showed specific nuclear signal in A1 and A3 spermatogonia, with a 10% false negative rate (Fig. 5F,G, $Cbx2^{Flox/Flox}$). We used A3 spermatogonia to assess the general mutation rate because A3 spermatogonia still robustly express *Cbx2*. After tamoxifen-induced deletion of *Cbx2*, *Cbx2* RNA-FISH showed that ~10% of A1 spermatogonia were homozygous for the *Cbx2* mutant, whereas ~40% of A3 spermatogonia were homozygous *Cbx2* mutant (Fig. 5F,G, $Rosa26\text{-}CRE^{ERT2}$; $Cbx2^{Flox/Flox}$, see red circles for mutants). This proportion of *Cbx2* mutants (~40%) was in line with the data from single-cell genotyping (Supplemental Fig. S5D). Overall, these data suggest that there was specific depletion of *Cbx2* mutant A1 spermatogonia.

Immunostaining of CCND2 in *Cbx2* mutant tubules also showed that CBX2 is needed for the production of A1 spermatogonia. We could not confidently tell *Cbx2* genotypes by immunostaining due to limited antibody sensitivity, so we performed experiments by inducing as complete a homozygous-null *Cbx2* mutation as possible using a mouse line in which one allele of *Cbx2* was already deleted (see the Materials and Methods). We estimate that up to ≥60% cells are *Cbx2*-null based on *Cbx2* DNA-FISH (Supplemental Fig. S6A,B and legends). Quantification of $CCND2^+$ cells at stage VII/VIII tubules by whole-mount immunostaining showed a significant decrease of $CCND2^+$ cells in the *Cbx2* mutant compared with control animals (Supplemental Fig. S5F,G). The number of preleptotene spermatocytes in the same stage VII/VIII tubules did not show significant differences (Supplemental Fig. S5H), suggesting that CBX2 function is specific to the production of $CCND2^+$ A1 spermatogonia. Notably, the phenotype of CBX2 depletion on A1 spermatogonia coincides with the strong up-regulation of CBX2 expression at the A1 stage in wild-type animals (Fig. 2C,D). We did not detect a significant increase in the number of apoptotic cells in the stage VI–VIII tubules where A-aligned-to-A1 transition happens (Supplemental Fig. S5I,J), suggesting that CBX2 function is not likely to be required for the survival of germ cells. We conclude that CBX2 is required for appropriate differentiation, specifically for the transition to the differentiating spermatogonia.

CBX2 represses genes active in spermatogonial stem cells in differentiating spermatogonia

Mutations in cPRC1 components often result in subtle or stochastic misexpression of target genes (Kundu et al. 2017; Kim and Kingston 2022). Therefore, we performed a deeper, bulk RNA-seq comparison between *Cbx2* wild-

type and *Cbx2* mutant c-KIT$^+$ spermatogonia to capture small changes of lowly expressed genes. From this comparison, we identified 436 up-regulated and 563 down-regulated genes by inducible knockout of *Cbx2* (Fig. 6A). Although the major role of PRC1 is the maintenance of gene repression, PRC1 can also mediate gene activation (Kondo et al. 2014; Maezawa et al. 2017). To determine whether any of these genes are directly regulated by CBX2, we compared the binding of CBX2 at their promoters using CBX2 CUT&RUN data. Only genes that were up-regulated in mutant cells, but not genes that were down-regulated, showed significantly higher levels of CBX2 binding at promoters when compared with 436 expression level-matched random genes (Fig. 6B; Supplemental Fig. S6C). This result suggests that CBX2 directly maintains repression of these up-regulated genes and that down-regulated genes may reflect secondary consequences, such as a delay in differentiation. These up-regulated genes normally had a relatively higher expression in SSCs and were down-regulated when SSCs differentiated to CBX2-expressing c-KIT$^+$ spermatogonia (Fig. 6C). On the other hand, down-regulated genes had a relatively higher expression in terminally differentiating spermatocyte stages (Fig. 6C). Thus, in irreversibly committed c-KIT$^+$ spermatogonia, CBX2 represses genes that are active in SSCs and subsequently down-regulated.

The CBX2 CaPS region is required for germ cell maintenance

CBX2 can both compact nucleosomal arrays and phase-separate, both activities that rely on the positive charge

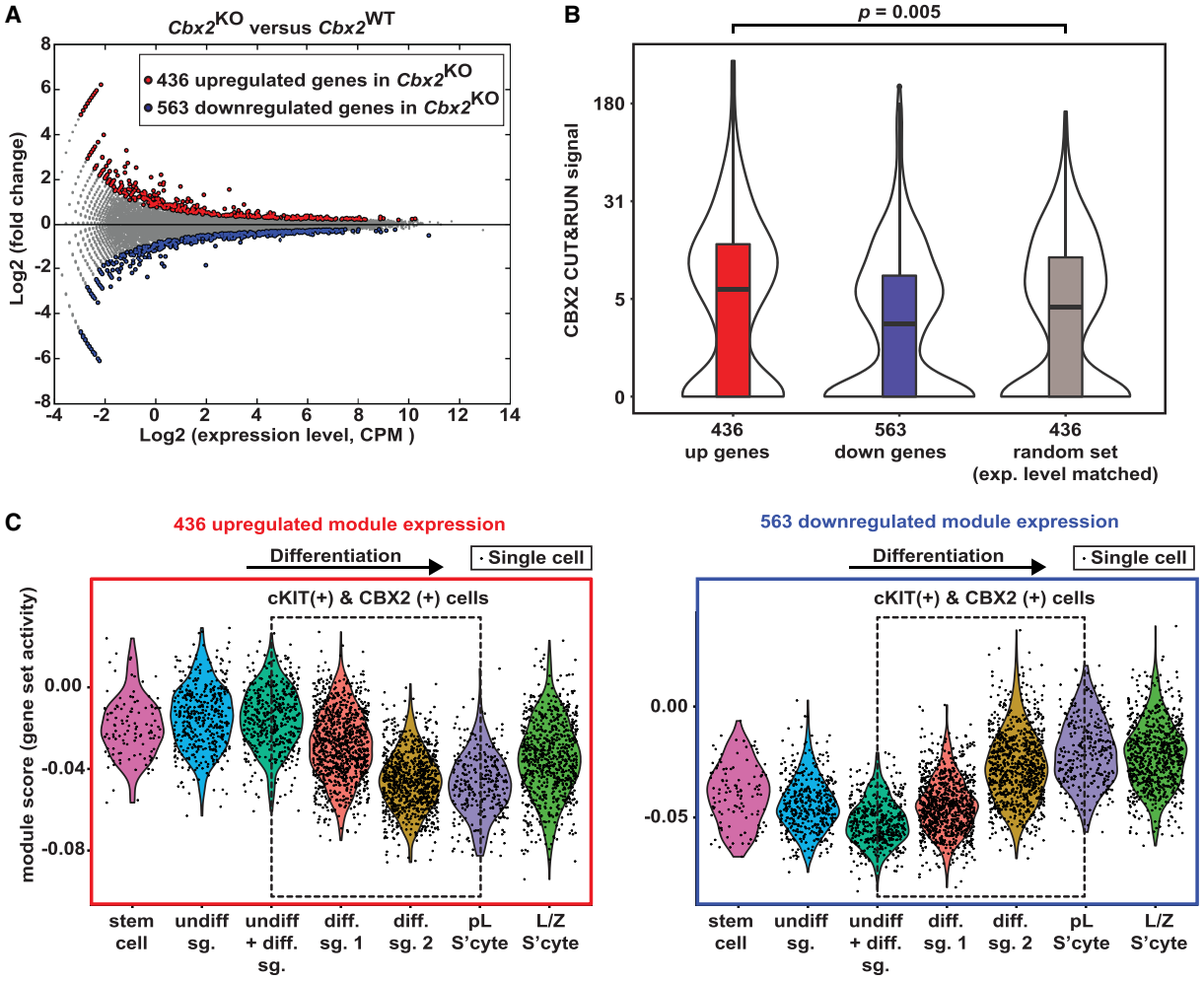

Figure 6. CBX2 represses genes active in spermatogonial stem cells in differentiating spermatogonia. (*A*) An MA plot showing differences between *Cbx2*^{WT} (*Rosa26-Cre*^{ERT2}; *Cbx2*$^{Flox/+}$, mock-injected) and *Cbx2*^{KO} (*Rosa26-Cre*$^{ERT2/+}$; *Cbx2*$^{\Delta/Flox}$, tamoxifen-injected). Red dots show up-regulated genes ($P < 0.05$), and blue dots show down-regulated genes ($P < 0.05$) (see the Materials and Methods). (*B*) Violin plots showing CBX2 CUT&RUN signal (background-corrected by subtracting IgG CUT&RUN signal) of up-regulated and down-regulated genes and 436 randomly chosen control genes matching expression levels of 436 up-regulated genes. *P*-values are based on Wilcoxon rank sum test. (*C*) Average expression levels of the 436 up-regulated genes or 563 down-regulated genes in *A* as a gene set per cell in single-cell clusters represented in Figure 2B. (sg) Spermatogonia, (S'cyte) spermatocyte, (undiff) undifferentiated, (diff) differentiating, (pL) preleptotene, (L/Z) leptotene/zygotene).

of the central "CaPS" (compaction and phase separation) region (Supplemental Fig. S1A). We examined the hypothesis that this region might be important for CBX2 function in spermatogenesis by using a knock-in mouse line in which the endogenous CaPS region of both CBX2 alleles was mutated. The replacement of 23 positively charged amino acids (Lys and Arg) of CBX2 with a neutral amino acid (Ala; referred to here as the *Cbx2*^{23KRA} mutant) (Supplemental Fig. S1A) in the CaPS region diminished polynucleosome compaction (Grau et al. 2011) and phase separation activities (Plys et al. 2019) in vitro and resulted in posterior transformation of axial skeletons in vivo (Lau et al. 2017). Using the CaPS region mutant, we tested whether this functional region of CBX2 played a role in adult tissue homeostasis during spermatogenesis. The CBX2^{23KRA} mutant does not disrupt other domains needed for chromatin targeting and for cPRC1 formation.

Cbx2$^{23KRA/23KRA}$ mice showed progressive defects in male germ cell maintenance as mice aged. Both heterozygous and homozygous *Cbx2*^{23KRA} mutant mice showed largely normal development and fertility, albeit with axial skeletal defects (Lau 2016). Consistent with the results from mESCs (Jaensch et al. 2021) and MEFs (Isono et al. 2013) showing that factors in addition to CaPS also are able to drive Polycomb body formation, spermatogonia from wild-type and *Cbx2*$^{23KRA/23KRA}$ mice did not show visible differences in CBX2-Polycomb puncta (Supplemental Fig. S7A). While *Cbx2*$^{23KRA/+}$ and *Cbx2*$^{23KRA/23KRA}$ mice had similar body weights when compared with wild-type siblings up to ~40 wk of age (Fig. 7A), the *Cbx2*$^{23KRA/23KRA}$ mutant mice had lower testis weights than their wild-type siblings as the mice got older, especially >30 wk (Fig. 7B,C). This result indicates a progressive defect in spermatogenesis as mice aged. Histological examination of testis sections of old (>30-wk-old) *Cbx2*$^{23KRA/23KRA}$ mutant mice revealed clusters of defective tubules that were devoid of all germ cells and only had Sertoli cells at the basement membrane (Fig. 7D,E,G). Five percent of tubules (median value) were devoid of germ cells in homozygous *Cbx2*$^{23KRA/23KRA}$ mutant mice, which was significantly higher than in wild-type siblings, which rarely showed germ cell-less tubules (Fig. 7F). Some tubules exhibited a "missing generation" phenotype (Lovasco et al. 2015). For example, some tubules lacked spermatocytes or spermatids (Fig. 7H,I), indicating that SSCs did not differentiate in one of previous differentiation cycles, potentially to preserve their declining numbers or due to problems in differentiation.

It is notable that only a fraction of tubules showed complete loss of germ cells, while adjacent tubules seemed to maintain normal spermatogenesis, which presumably contributed to the sustained fertility of these mice (Fig. 7E). To probe whether there are subtle defects in the seemingly normal tubules in the *Cbx2*$^{23KRA/23KRA}$ mice, we counted the numbers of A spermatogonia and preleptotene and zygotene spermatocytes in stage VII/VIII and XII tubules using histological sections from old (>30-wk-old) mice (Supplemental Fig. S7B,C). In all cases, there were no striking differences between wild-type and *Cbx2*$^{23KRA/23KRA}$ mutants in the number of germ cells (Supplemental Fig. S7D–G). However, the number of A_{undiff} and A1 spermatogonia per tubule section showed a decrease in median number, with *Cbx2*$^{23KRA/23KRA}$ mice having more tubule sections without any spermatogonia (Supplemental Fig. S7D). No such decrease was observed in other cell types in the lineage (Supplemental Fig.

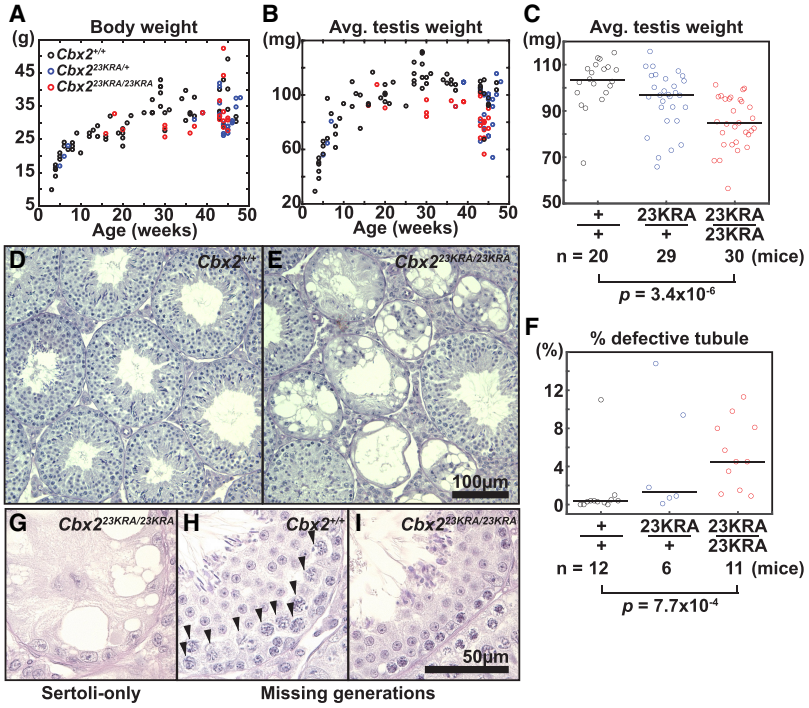

Figure 7. Spermatogenesis defects in CBX2 CaPS region mutant mice. (*A*,*B*) Body weight (*A*) and average testis weight (*B*) of wild-type and *Cbx2*$^{23KRA/+}$ and *Cbx2*$^{23KRA/23KRA}$ mutant mice at the time of euthanasia. (*C*) Quantification of average testis weights of aged (>30-wk-old) mice. The *P*-value is based on Wilcoxon rank sum test. (*D*,*E*) Representative images of hematoxylin-PAS-stained testis sections of sibling wild-type (*D*) and *Cbx2*$^{23KRA/23KRA}$ mutant (*E*) mice. (*F*) Quantification of the percentage of tubules with defects in germ cell maintenance in wild-type and *Cbx2*$^{23KRA/+}$ and *Cbx2*$^{23KRA/23KRA}$ mutant mice. The *P*-value is based on Wilcoxon rank sum test. (*G*–*I*) Representative images of hematoxylin-PAS-stained testis sections showing Sertoli cell-only (*G*), missing generation phenotypes (*H*,*I*), and lacking spermatocytes (*I*; arrowheads in *H*).

S7E–G). These data indicate that the regulation of the ratio of spermatogonia to spermatocytes is mostly normal except for an imbalance in A_{undiff}/A1 spermatogonia distribution. Over time, this imbalance might contribute to defects in spermatogenesis. In addition, this result suggests that disruption of the CaPS region in CBX2 likely plays a similar role as to the deletion of CBX2, which showed a significant depletion of A1 spermatogonia. Consistently, genes derepressed in *Cbx2*^{KO} spermatogonia (Fig. 6A) also tend to be up-regulated in *Cbx2*$^{23KRA/23KRA}$ spermatogonia based on a bulk RNA-seq comparison of c-KIT^{+} spermatogonia (Supplemental Fig. S7H). Notably, there were no significant differences in binding of CBX2 or enrichment of H3K27me3 and H2AK119Ub1 modifications at 708 CBX2-bound genes between wild-type and *Cbx2*$^{23KRA/23KRA}$ c-KIT^{+} spermatogonia by CUT&RUN (Supplemental Fig. S7I). Thus, for long-term tissue homeostasis, a nonenzymatic activity of CBX2-cPRC1 is critical for preventing stochastic loss of germ cells and hence maintenance of spermatogonial stem cells.

Discussion

Our characterization of the role for the CBX2 subunit and for its main functional region during spermatogenesis advances the understanding of how PcG regulates cell fate transition in a tissue-specific stem cell lineage in an animal. CBX2 is up-regulated in a cell type-specific manner as spermatogonial stem cells initiate differentiation and is required for the repression of genes active in SSCs. CBX2 forms nuclear condensates with its target genes, and its region responsible for compaction and phase separation is required specifically for male germ cell maintenance (Fig. 8). We propose that the ability of CBX2-cPRC1 to alter chromatin structure is critical for a specific step in spermatogenesis (the formation of CCND2^{+} A1 spermatogonia) and for maintenance of a key adult stem cell lineage.

The balance between the maintenance of stem cells and commitment to differentiation is a critical regulatory point for tissue homeostasis. Some PcG proteins are specifically expressed and required in certain adult stem cell types (Flora et al. 2021). In contrast, we found that CBX2 expression was relatively low in spermatogonial stem cells, was up-regulated as stem cells initiate differentiation, and was necessary for the repression of genes active in SSCs. Therefore, in the male germ cell lineage, CBX2-cPRC1's most prominent role is in committed progenitor cells, specifically A1 spermatogonia, and not in stem cells. This CBX2 expression pattern is reminiscent of its expression during differentiation in cultured mouse embryonic stem cells (mESCs), in which CBX2 is up-regulated as mESCs differentiate into embryoid bodies or neural progenitor cells (Morey et al. 2012; O'Loghlen et al. 2012). In addition, *Cbx2* was shown to be up-regulated in differentiating human bone marrow cells but not in immature cells (Lessard et al. 1998). Thus, CBX2 expression is associated with lineage commitment in diverse developmental contexts. As CBX2 is required to repress SSC genes, *Cbx2* mutant A-aligned spermatogonia may be closer to the SSC state and less competent to respond RA to become A1 spermatogonia. While the exact mechanism for how the number of A1 spermatogonia is reduced in *Cbx2* mutant animals remains to be elucidated, the key conclusion is that CBX2 is not a general factor required for all dividing cells but rather regulates a specific developmental transition step.

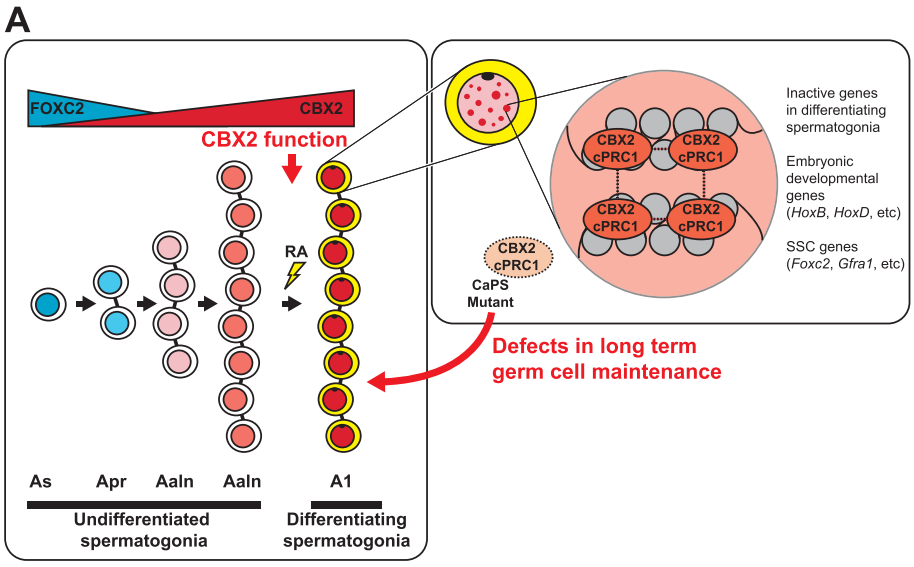

Figure 8. A model of CBX2 function at the exit from the SSC state. CBX2 expression is up-regulated as A-single or A-paired spermatogonia differentiate to A-aligned spermatogonia. CBX2 expression further increases at A1 spermatogonia when the cells irreversibly commit to differentiation. CBX2 function is required specifically for the production of A1 spermatogonia. In differentiating spermatogonia, CBX2 forms Polycomb bodies that encompass its target genes that need to remain repressed. Disruption of the CaPS region of CBX2 results in defects in the long-term maintenance of germ cells.

Phase separation has been proposed to play a key role in the maintenance of repressive states based on studies of the heterochromatic protein HP1 (Larson et al. 2017; Strom et al. 2017) and previous analysis of CBX2 and PcG function (Plys et al. 2019; Tatavosian et al. 2019). There is scant information concerning the extent to which phase separation occurs in living adult animals and the extent to which it might contribute to the maintenance of stably differentiated tissues. We show that in testes there is overlap of puncta containing CBX2-PRC1 and *HoxD* and *HoxB* target genes. Therefore, these puncta, previously shown to be present in embryos (Grimaud et al. 2006) and cultured cells (Satijn et al. 1997; Saurin et al. 1998; Isono et al. 2013), also exist in an adult animal tissue and are coresident with target genes. Although the *HoxD* locus did not overlap with CBX2 or RING1B signal in ~30% of the images, this degree of nonoverlap is similar to what was observed in MEFs, showing ~20% of nonoverlap between PCGF2 (MEL-18) and *HoxB* loci (Isono et al. 2013). This degree of nonoverlap might be technical, as heat applied to denature the DNA duplex disrupts immunostaining signal patterns and intensity. Alternatively, it might be that in certain cell cycle phases (for example, S phase), Polycomb target loci may temporarily be displaced from Polycomb bodies.

Aged mice with a mutation in the region required in vitro for both phase separation and chromatin compaction ("CaPS" region) developed sporadic empty tubules in the testes but still had visible puncta of PRC1 in spermatogonia (Supplemental Fig. S7A). Formation of Polycomb bodies in the CaPS mutant in vivo is consistent with previous data in cell culture (Jaensch et al. 2021), and other components of PRC1, such as the PHC proteins, are known to be able to phase-separate and oligomerize (Isono et al. 2013; Seif et al. 2020). Whether the condensates driven by PHC function have properties similar to the condensates that also contain wild-type CBX2 is an open question. In addition, paralogous CBXs can complement CBX2 function. For example, *Cbx4* and *Cbx8* were expressed in differentiating spermatogonia (Supplemental Fig. S2A) and were up-regulated in *Cbx2* KO embryos (Supplemental Fig. S1C). Different CBXs have distinct diffusion properties in the nucleus (Zhen et al. 2016). Thus, even though Polycomb bodies are still present in the *Cbx2* CaPS mutant testes, changes in the contributions of different CBXs and PHCs may alter biophysical properties of these condensates. This, in turn, may decrease the effectiveness of cPRC1 in driving memory of cell fate but does not eliminate memory. A similar phenomenon was observed with a yeast Polycomb-like protein, Ccc1, where one type of KRA mutant still formed condensates but had altered physical properties and gene silencing defects (Lee et al. 2023).

In aged *Cbx2* CaPS region mutant mice, some tubules show a complete loss of germ cells, implying a loss of SSCs. As CBX2 was required for commitment to A1 cells when acutely depleted, it is counterintuitive that the precursor SSCs are also lost in the *Cbx2* CaPS mutant testes. However, the depletion of germ cells in *Cbx2* CaPS mutant testes only becomes noticeable after 30 wk (Fig. 7), which corresponds to up to 20 cycles of new A1 spermatogonia production events. Disruption of the initial phase of differentiation (the production of A1 spermatogonia) might generate a feedback loop in which, over time, accumulation of stress could cause some tubules to lose SSCs. Similarly, the knockout of another PcG gene, *Eed*, did not alter the initial hematopoietic stem cell (HSC) establishment in fetal livers but showed defects in their differentiation and ultimately led to their depletion due to exhaustion (Xie et al. 2014). CBX2 may have an additional direct role in SSC maintenance. However, given its strong up-regulation upon differentiation, we hypothesize that the loss of SSC is a secondary consequence of cumulative long-term defects in differentiation. Such feedback regulation of undifferentiated spermatogonia by differentiating spermatogonia was reported in other rodent species (de Rooij et al. 1985). In the future, direct comparative analyses will be informative to resolve the exact roles of different *Cbx2* mutations. For example, transplantation of *Cbx2* wild-type, knockout, and CaPS mutant SSCs into germ cell-depleted testes is one way to compare the cellular and physiological phenotypes within the same environment.

Another noticeable feature of the *Cbx2* CaPS mutant is that some tubules show complete loss of germ cells, while neighboring ones maintain seemingly normal spermatogenesis. Total output of sperm is regulated in part by overproduction of undifferentiated spermatogonia followed by regulated proliferation, migration, and apoptosis of differentiating spermatogonia (de Rooij and Russell 2000; Yoshida et al. 2007). Therefore, even if there is a reduction in the number of SSCs, the remaining SSCs in principle can support normal spermatogenesis until the number falls below critical levels within a specific tubule. This all-or-nothing phenotype was also observed in mutants affecting SSC maintenance, such as *Zbtb16* (Buaas et al. 2004; Costoya et al. 2004). The stark difference in the penetrance between tubules might arise due to the combined impacts of the robust nature of spermatogenesis and the stochastic nature of PcG gene mutants (Kim and Kingston 2022).

Conclusion

PcG genes are frequently dysregulated in human cancers and aging. Chemical inhibitors of PcG function have been developed to use chromatin pathways to reverse such conditions. However, to provide effective intervention, it is essential to understand how PcG dysfunction is involved in complex processes, such as the decline of tissue function. We demonstrate that CBX2 acts at the exit from the spermatogonial stem cell state for the commitment of differentiation, and the region required for compaction and phase separation is critical for the long-term maintenance of the lineage. Thus, the structural activity of cPRC1 driven by CBX2 is crucial for proper developmental transitions in the male germline and for maintenance of the complete germline machinery during aging. It will be important to investigate different biochemically defined CBX2 loss- or gain-of-function mutations and their impact on compaction and phase separation in cell fate transitions during adult tissue homeostasis.

Materials and methods

Mice

All animal procedures were conducted in accordance with protocols approved by the Massachusetts General Hospital Institutional Animal Care and Use Committee (IACUC, protocol no. 2015N000072), and animals were cared for according to the requirements of the National Research Council's Guide for the Care and Use of Laboratory Animals.

The floxed $Cbx2^{Flox}$ mouse line was generated from the parental "targeted trap" line [Cbx2tm1a(KOMP)Wtsi; referred to here as $Cbx2^{tm1a}$] that was originally produced by the Knockout Mouse Project (KOMP) (Skarnes et al. 2011). Aliquots of cryopreserved sperm ($Cbx2^{tm1a}$) were obtained from the University of California, Davis, Mouse Biology Program KOMP, and in vitro fertilization was performed by Charles River Laboratories. Rederived $Cbx2^{tm1a}$ females were crossed to male mice expressing FLP recombinase [C57BL/6N-Tg(CAG-Flpo)1Afst/Mmucd; stock no. 036512-UCD] to excise the LacZ reporter trap flanked by FRT sites to make "conditional-ready" $Cbx2^{Flox}$ mice (also referred to as $Cbx2^{tm1c}$ per the European Mouse Mutant Cell Repository nomenclature). To produce an inducible *Cbx2* deletion line, $Cbx2^{Flox}$ mice were crossed to the mice expressing CRE recombinase responsive to tamoxifen [R26-CreERT2; full genotype: B6.129-Gt(ROSA)26Sortm1(cre/ERT2)Tyj/J; Jackson Laboratory 008463]. An inducible *Cbx2* deletion line with one deleted *Cbx2* allele (*R26-CreERT2; Cbx2*$^{\Delta/Flox}$) was produced by crossing $Cbx2^{\Delta/+}$ males to *R26-CreERT2/+; Cbx2*$^{Flox/Flox}$ females. $Cbx2^{Flox}$ and its derivative lines were backcrossed to C57BL/6J mice more than five times. The $Cbx2^{23KRA}$ strain (Lau et al. 2017) is available through the Mutant Mouse Resource and Research Center (MMRRC; B6J.Cg-Cbx2tm1.1Rek/Mmnc; stock no. 050534-UNC). The $Cbx2^{\Delta}$ strain has a deletion (mm10, chr11:119,028,119–119,028,164) by CRISPR/Cas9 that introduces a premature stop codon after amino acid 171. For the $Cbx2^{23KRA}$ strain, only nonstud males were used for aged phenotyping experiments to minimize the potential influence of the presence of females on spermatogenesis (Schmidt et al. 2009). All experiments were done with male mice between 8 and 20 wk old, except aged mouse phenotyping in Figure 7, D–F, and Supplemental Figure S7, B–G, where 30- to 45-wk-old mice were used. $Cbx2^{23KRA}$ and $Cbx2^{\Delta}$ strains were backcrossed to C57BL/6J more than eight times. All C57BL/6J mice used for backcross were obtained from the Jackson Laboratory (stock no. 000664). PCR primers for genotyping are listed in Supplemental Table S1.

Tamoxifen administration

Tamoxifen (Sigma-Aldrich T5648) was dissolved in corn oil (Spectrum Chemical CO136) to a final concentration of 20 mg/mL by incubating the mixture overnight at 37°C while rotating. Dissolved tamoxifen was filtered, and aliquots for daily use were stored in sterile tubes and kept for up to 4 d at 4°C. For the *Cbx2* amplicon single-cell RNA-seq experiments, 150 µL of warmed (room temperature) tamoxifen/corn oil was injected intraperitoneally daily for three consecutive days. For CCND2 and cleaved-Caspase 3 immunostaining experiments, 200 µL of warmed tamoxifen/corn oil was injected intraperitoneally daily for four consecutive days to make as complete a *Cbx2* mutant as possible.

Generation of the $Cbx2^{HA}$ strain

To knock in HA epitope tags at the N terminus of the *Cbx2* gene, guide RNA (Synthego), single-stranded repair oligo (Genewiz), and Cas9 enzyme (Alt-R S.p. Cas9 nuclease V3; Integrated DNA Technologies 1081058) were electroporated into B6 mouse zygotes by the Genome Modification Facility at Harvard University. DNA sequences are listed in Supplemental Table S1. A predicted 295-bp knocked-in DNA fragment (232 bp for WT) was PCR-amplified from genomic DNA of targeted pups. PCR fragments from four pups (out of 13) with the expected knock-in size were deep-sequenced by the Massachusetts General Hospital Center for Computational and Integrative Biology DNA Core (CRISPR amplicon sequencing). The following 63-bp sequence was knocked in right after the ATG start codon: TATCCATACGATGTTCCTGAC TATGCGGGCTATCCCTATGACGTCCCGGACTATGCAGG ATCC (inserted right after position chr11:119023111, mm10). One Gly linker (underlined) was placed between HA sequences, and one GlySer linker (underlined) was placed between the 2xHA and CBX2 proteins (YPYDVPDYAGYPYDVPDYAGS). Three mice (two HA/deletion males and one HA/HA female) contained the correctly targeted allele. Two founder males sired progenies. Homozygous $Cbx2^{HA/HA}$ males were produced by crosses between the progeny of the two different founders to minimize potential off-target mutations becoming homozygous. Targeted strains were backcrossed three times to C57BL/6J mice at the time of immunostaining and CUT&RUN experiments.

Testis dissociation to obtain single cells

Testes were obtained, and tunica albuginea membrane was removed. Released seminiferous tubules were gently separated in PBS. Roughly separated tubules were incubated in collagenase type IV in 1 mg/mL DMEM (5 mL for one testis pair; Stem Cell Technologies, Inc., 07909) at 37°C while rotating. After an initial 10-min incubation, the collagenase solution with released interstitial cells was removed, and the same volume of fresh collagenase solution was added to the seminiferous tubules. Tubules were further dissociated by incubating for another 10 min at 37°C with occasional stirring and pipetting up and down. Dissociated tubules were centrifuged at 300*g* for 3 min. The supernatant was removed, and trypsin (Thermo Fisher Scientific 12605010) solution was added to make a single-cell suspension. After 5 min of trypsin incubation at 37°C with occasional mixing, dissociated cells were passed through 40-µm-wide cell strainers. One volume of 4°C DMEM (Thermo Fisher Scientific 11960044) with 10% fetal bovine serum (Sigma-Aldrich F2442) was added, and the single-cell suspension was centrifuged at 400*g* for 6 min. Cell pellets were resuspended in 4°C DMEM with 10% FBS.

Fluorescence-activated cell sorting (FACS)

Cells were resuspended in PBS at 4°C at ~1×10^7/mL concentration. Cells were first stained with cell viability dye Zombie Green (BioLegend 423111) for 20 min at room temperature. After one wash with PBS (plus 0.5% [w/v] BSA), cells were incubated with cell surface antibodies in PBS (plus 0.1% [w/v] BSA) for 30–60 min at 4°C. Antibody product and dilution information are listed in Supplemental Table S2. After antibody incubation, cells were washed with 50 mL of 4°C PBS once and then resuspended in PBS (plus 0.1% [w/v] BSA) at ~1×10^7/mL concentration. FACS was performed with BD FACS Melody.

Preparation of cell and tissue lysates for immunoblotting

Dissociated single cells or tissue material were dissolved in SDS tissue lysis buffer (20 mM Tris-HCl at pH 8.0, 135 mM NaCl, 10% glycerol, 1% Igepal, 1% SDS, 5 mM EDTA). One microliter of benzonase (25,000 U; Millipore 71205) was added per 200 µL of lysis buffer. Tissue pieces were homogenized by passing through

23-gauge and 25-gauge needles consecutively at least 10 times. Cell and tissue lysates were incubated for ~15 min at room temperature until the lysates were no longer viscous. If the lysates were still viscous, they were sonicated with a Bioruptor at "high" setting for 4 min (30 sec on/30 sec off). Whole-cell or tissue lysates were used for immunoblotting without further separation by centrifugation.

Western blot

Cell or tissue lysates (10–20 µg) were mixed with 5× Western loading buffer and incubated for 5 min at 95°C. Samples were then loaded onto 4%–20% polyacrylamide gels in Western running buffer (25 mM Tris, 192 mM glycine, 0.1% [w/v] SDS) at a constant ~120 V for 2~3 h. After separation, proteins were transferred to PVDF membrane (Fisher Scientific IPFL00010) in Western transfer buffer (25 mM Tris, 192 mM glycine, 20% [v/v] methanol) at a constant 45 mA overnight for a total 400 Vh. After confirming the transfer with Ponceau staining, membranes were washed once with wash buffer (PBS, 0.1% Tween 20) and incubated in a blocking buffer (PBS, 0.1% Tween 20, 5% [w/v] skim milk) for 30 min at room temperature. Membranes were incubated with primary antibodies with the desired concentrations in the incubation buffer (PBS, 0.1% Tween 20, 2% [w/v] skim milk) overnight at 4°C. The concentrations of antibodies and their sources are listed in Supplemental Table S2. Membranes were washed three times in the wash buffer (PBS, 0.1% Tween 20) and incubated with secondary antibodies conjugated with HRP in the incubation buffer overnight at 4°C. Membranes were washed three times and developed with ECL solution (Thermo Scientific 1859698 and 1859701).

Tissue preparations for RNA in situ hybridization, immunostaining, and histology

Dissected testes and epididymides were fixed in >10 mL of 4% formaldehyde in PBS (for immunostaining or in situ hybridization) at 4°C or in Bouin's fixative (for hematoxylin/PAS staining) overnight at room temperature with rocking. Testes were cut in half the next day and fixed with the same fixatives for another 2 h. After washing with water, testes and epididymides were dehydrated with successive incubation in 30%, 50%, and 70% ethanol for 1 h each. Fixed and dehydrated testes and epididymides were paraffin-embedded and cut to 5-µm thickness for subsequent experiments.

Immunostaining of testis sections

Cut sections on microscope slides were baked in an oven for 1 h at 60°C. The paraffin was removed by incubating the sections three times for 10 min in xylene, and residual xylene was washed away by incubating three times in 100% ethanol for 5 min. Samples were subsequently rehydrated by incubating in 95%, 85%, and 70% ethanol for 3 min each and rinsed with >4 L of water. Deparaffinated samples were antigen-retrieved by incubating in boiling retrieval buffer (10 mM sodium citrate at pH 6.0, 0.05% [v/v] Tween-20) for 10 min. Boiled slides were cooled and washed with >4 L of water. Samples were incubated with a blocking buffer (3% [w/v] BSA, 0.05% [v/v] Triton X-100, PBS) for 30 min at room temperature. Samples were incubated with primary antibodies in a blocking buffer overnight at 4°C and washed three times with PBST (0.05% [v/v] Triton X-100, PBS). Primary antibody information is listed in Supplemental Table S2. Samples were then incubated with secondary antibodies in a blocking buffer overnight at 4°C and washed four times with PBST. The second wash was done with PBST with Hoechst 33342 (final concentration 1 µg/mL; Life Technologies H3570). Both primary and secondary antibody incubations were done in a humidified chamber. Coverslips were put on top of sections with mounting media (VectaShield, Vector Laboratories H-1000) and sealed with nail polish (Fisher Scientific 72180). Slides were imaged with a Nikon 90i Eclipse epifluorescence microscope equipped with an ORCA-ER-1394 CCD camera (Hamamatsu).

Immunostaining of testis tubules

Testis tubules were gently separated in 4°C PBS. Dissociated tubules were fixed in 4% formaldehyde in PBS for 15 min at room temperature with occasional rocking. Fixed tubules were then quickly washed twice with PBS, incubated in 100 mM Tris (pH 8.0) for 10 min to quench unreacted formaldehyde, and washed twice with PBS. Fixed tubules were transferred to 10-cm Petri dishes in PBST (0.1% Triton X-100). Tubules were cut into ~1-mm-long pieces under a dissection microscope. When imaging stage VI–VIII tubules, "dark zone" tubules were collected because in stage VII, spermatids move toward the lumen showing characteristic dark patterns in the middle of tubules (Kotaja et al. 2004). More than 30 pieces of ~1-mm-long tubules were transferred to test tubes using wide-bore tips and blocked in PBST BSA (0.05% Triton X-100, 3% [w/v] BSA) for >15 min. Tubules were then incubated with primary antibodies for two nights at 4°C, washed three times with PBST (0.05% Triton X-100), incubated with fluorophore-conjugated secondary antibodies overnight, and then washed four times with PBST (0.05% Triton X-100). For the second wash, Hoechst 33342 (final concentration 1 µg/mL; Life Technologies H3570) was added to label nuclei. Washed tubules were mounted on glass slides, arranged on the slides in a nonoverlapping manner, and mounted with mounting media (VectaShield, Vector Laboratories H-1000). Tubules were imaged with a Leica TCS SP5 confocal microscope with at least 2× line averaging for 1024 × 1024 pixels. All settings, including laser intensity, gain, offset, and pinhole size, were kept constant between the samples being compared. Pixel intensity was measured by manually selecting spermatogonial nuclei with "oval selections" (6-µm diameter) in Fiji (version 1.53c) (Schindelin et al. 2012).

Immunostaining of dissociated cells on coverslips

Coverslips (12-mm circles, thickness 1; Fisher Scientific 72231-01) were incubated with poly-D-lysine (R&D Systems 3439-100-01) for >5 min prior to the cell attachment. One milliliter of dissociated cells from testes (>1×10^5 cells per well) in PBS was applied on the coverslips in a 24-well plate. The plate was briefly centrifuged at 80*g* for 1 min. The attached cells were fixed with 1% (v/v) formaldehyde in PBS for 15 min at room temperature. After fixation, coverslips were washed twice with PBS and once with PBST. Coverslips were blocked and incubated with antibodies in 24-well plates as specified in the sections detailing immunostaining of testis. Mounted coverslips were imaged with a Leica TCS SP5 confocal microscope with at least 2× line averaging for 512 × 512 pixels.

CBX2 antibodies

N-terminal FLAG epitope-tagged nearly full-length CBX2 (FLAG-CBX2-ΔCbox, amino acids 1–485) protein was used as an antigen. C-terminal Cbox was deleted to prevent CBX2 from degradation when overexpressed without its binding partner, RING1B. CBX2 protein was expressed in Sf9 cells using the baculovirus system and affinity-purified from nuclear extracts using agarose beads

coupled with the M2 anti-FLAG antibody (Sigma-Alrich A2220). One milligram of 1 mg/mL purified CBX2 protein was injected into two rabbits for initial immunization. Subsequently, 0.2 mg of 0.5 mg/mL purified CBX2 protein was injected for boosts at days 14, 21, 49, and 77. Final antisera were obtained on day 91. Antibodies against CBX2 were affinity-purified using the Affi-gel-coupled (Affi-Gel 10, Bio-Rad 1536099) FLAG-CBX2-ΔCbox, concentrated, and stored in PBS with 10% glycerol. All rabbit experiments were done in Cocalico Biologicals with a USDA research license and animal welfare assurance with the National Institutes of Health (http://www.cocalicobiologicals.com/antibodies.html).

RNA in situ hybridization

For tissue sections, *Cbx2* in situ hybridization on testis sections was performed using the RNAScope (Advanced Cell Diagnostics 322300) based on the manufacturer's protocol. Antigen retrieval was performed for 10 min in a boiling antigen retrieval buffer. *Cbx2* probes targeted the 541–1606 region of transcript NM_007623.3. Images were acquired with a Leica DM5000B microscope.

For whole-mount tubules, fixed seminiferous tubule fragments were collected as described in "Immunostaining of Testis Tubules." To analyze A1 spermatogonia in stage VII/VIII tubules and A3 spermatogonia in stage XII tubules, "dark zone" and "pale zone + weak spot" tubules were collected (Kotaja et al. 2004). Collected tubule fragments were permeabilized in cold 70% ethanol for at least 1 h at 4°C. In situ hybridization was performed based on the protocol from Molecular Instruments with the following modifications. Hybridization buffer containing 4 nM each probe set was added directly to preamplification buffer because the tubule segments did not sink and it was hard to remove preamplification buffer. Hybridization was performed in a hybridization oven for >12 h at 37°C. Amplification was performed with 60 nM each amplifier oligo for >12 h at room temperature. For the second wash, Hoechst 33342 (final concentration 1 µg/mL; Life Technologies H3570) was added in the wash buffer to label nuclei. Tubules were imaged with a Leica TCS SP5 confocal microscope with at least 2× line averaging for 1024 × 1024 pixels. Five images were acquired in 1-µm intervals for each acquisition and processed to make a combined Z-stack using ImageJ's "Z projection" with "maximum intensity." All settings, including laser intensity, gain, offset, and pinhole size, were kept constant between the samples being compared.

Generation of DNA-FISH and RNA-FISH probes

For DNA-FISH, *HoxD* (mm10, chr2:74653050–74762090) and gene desert (mm10, chr11:37675694–38150801) probes were Alexa 647-labeled Oligopaint probes used in the previous study (Kundu et al. 2017) and generated based on the published protocol (Beliveau et al. 2012). *HoxB* (mm10, chr11:96349820–96368979) and the *Cbx2* floxed region (mm10, 119023798–119026717) were visualized using SABER-FISH, and the probes were generated based on the published protocol (Kishi et al. 2019) with the following modifications. The primer exchange reaction (PER) was performed for at least 3 h. The resulting probe concatemer length was verified using agarose gel electrophoresis with EtBr after making the concatemer part of the probes double-stranded by hybridizing nonfluorescent imager oligos. SABER-FISH oligo sequences are listed in Supplemental Table S1.

For RNA-FISH, HCR probe sets against *Ccnd2* (NM_009829.3) and the *Cbx2* floxed region (mm10, 119023798–119026717) were designed by Molecular Instruments. Thirty probes were designed per target. *Ccnd2* probes were coupled with amplifier B2, and *Cbx2* probes were coupled with amplifier B3.

Coimmunofluorescence staining DNA-FISH

FACS-sorted germ cells were attached to the coverslips and immunostained with the desired antibodies with the staining protocol described in "Immunostaining of Dissociated Cells on Coverslips." After staining, cells were refixed with 4% formaldehyde in PBS for 15 min. Coverslips were then washed twice with PBS and incubated with RNase A (Qiagen 19101) in PBS for 1 h at 37°C. After RNA removal, coverslips were dehydrated by successively incubating in 70%, 85%, 95%, and 100% ethanol for 1 min each. Dried coverslips were incubated with FISH hybridization buffer (50% [v/v] formamide, 2× SSC, 10% [v/v] dextran sulfate, 100 ng/µL fragmented salmon sperm DNA, 5 pmol of target probe). After DNA denaturation by incubating coverslips for 10 min at 78°C in a thermocycler, coverslips were then incubated in the humidified chamber overnight at 42°C. The next day, coverslips were washed four times with 2× SSC. The second wash was done with 2× SSC with 1 ng/µL Hoechst 33342 (Life Technologies H3570). After the final wash, the coverslips were mounted on slides with mounting medium (Vector Laboratories H-1000). Mounted coverslips were imaged with a Leica TCS SP5 confocal microscope with at least 2× line averaging 512 × 512 pixels.

Quantification of germ cells in histological sections

Seminiferous tubule stages were determined based on characteristic cellular organizations (Ahmed and de Rooij 2009) after periodic acid Schiff (PAS) and hematoxylin staining of Bouin-fixed testis sections. Spermatogonia (A1 and undifferentiated) and preleptotene spermatocytes were counted in stage VII/VIII tubules. Spermatogonia (A3 and undifferentiated) and zygotene spermatocytes were counted in stage XII tubules. The size of the tubule perimeter was measured to normalize cell numbers to a standard tubule size. Only the sections cut perpendicular to the tubule axis were counted to have a consistent number of germ cells at the basement membrane for a given tubule perimeter. Cell numbers from at least 15 stage VII/VIII and 10 stage XII tubules were counted per animal from two regions of a testis.

RNA-seq

c-KIT$^+$ spermatogonia were isolated as described in "Testis Dissociation to Obtain Single Cells" and "Fluorescence-Activated Cell Sorting (FACS)." More than 100,000 c-KIT$^+$ cells were isolated and centrifuged to remove sorting buffer. Cell pellets were snap-frozen in liquid nitrogen and stored at −80°C. RNA was isolated using Trizol-based phase separation, followed by column-based purification (RNeasy mini, Qiagen 74104). We used SMART-seq mRNA LP (Takara 634768) following the manufacturer's manual to make the RNA-seq libraries for the $Cbx2^{KO}$ experiments. Cells from two control ($R26\text{-}Cre^{ERT2}$; $Cbx2^{Flox/+}$, mock-injected) and two experimental ($R26\text{-}Cre^{ERT2/+}$; $Cbx2^{\Delta/Flox}$, tamoxifen-injected) animals were used. Equal amounts of total RNA (20 ng) were used as the starting material for each library. cDNA was amplified with seven PCR cycles. Equal amounts of cDNA (1.3 ng) were used for library preparation. Eleven cycles of library-amplifying index PCRs were performed.

We used SMARTer stranded total RNA-seq kit v2 (Takara 634411) following the manufacturer's manual to generate RNA-seq libraries for $Cbx2^{23KRA}$ experiments. Cells from five control ($Cbx2^{+/+}$) and five experimental ($Cbx2^{23KRA/23KRA}$) animals were used. cDNA was amplified with five PCR cycles. Subsequently, ribosomal cDNA was depleted, and unfragmented remaining cDNA was indexed and amplified with 16 PCR cycles.

Single-cell RNA-seq

We used Chromium single-cell 3′ library and gel bead kit v2 (10X Genomics 120267) for single-cell RNA-seq from wild-type adult testes. Testes were dissociated as described in "Testis Dissociation to Obtain Single Cells." Dissociated cells were diluted to 1000 cells/µL, and a total of 5200 cells (5.2 µL) was loaded into the Chromium controller to obtain RNA-seq profiles of ~3000 cells. After producing emulsions encapsulating gel beads and cells, reverse transcription and 12 cycles of PCR were performed to produce cell-barcoded amplified cDNA. Illumina sequencing-ready libraries were produced from 200 ng of the amplified cDNA based on the manufacturer's protocol. Twelve cycles of library amplification indexing PCR were performed.

Genotyping of Cbx2 amplicon from single-cell RNA-seq

Single-cell analysis with targeted genotyping was done by adapting "genotyping of transcriptome" (GoT) (Nam et al. 2019) and V(D)J region amplification of T or B cell receptor protocol by 10X Genomics. We aimed to make specific *Cbx2* amplicons from cell-barcoded cDNA to amplify cDNA fragments and sequence exon5 junctions to distinguish wild type (exon4 spliced to exon5) and mutant (exon2 spliced to exon5 after the deletion of exon3,4) for specific cell barcodes. c-KIT$^+$ spermatogonia were sorted to a concentration of ~300~600 cells/µL, and ~8000 cells were loaded into the Chromium controller. Single-cell barcoded cDNA was made with Chromium Next GEM single-cell 5′ reagent kits (10X Genomics 1000265) based on the manufacturer's protocol with 14 PCR cycles of cDNA amplification. We used 5′ barcoding instead of 3′ barcoding because deleted exons of *Cbx2* were close to the 5′ end of the gene. Illumina sequencing-ready libraries were produced from 50 ng of the amplified cDNA based on the manufacturer's protocol. Fourteen cycles of library amplification indexing PCR were performed.

To generate *Cbx2* amplicons, we performed nested PCRs to amplify *Cbx2*-specific cDNAs with cell barcodes. In the second PCR step of the nested PCR, *Cbx2*-specific primer that had a partial Illumina read2 sequence was used. The *Cbx2*-specific second nested primer also contained "stagger" sequences between the *Cbx2*-specific region and partial read2 to increase library complexity for accurate base calls during Illumina sequencing. We confirmed the amplification of the correct-sized bands corresponding to wild-type and deleted *Cbx2* amplicons by agarose gel electrophoresis. The amplified bands were excised and gel-purified. Index PCR was performed to make the final Illumina-compatible libraries with unique indices with 10X Genomics-provided index PCR primers. *Cbx2* amplicon libraries were pooled with standard 10X Genomics single-cell gene expression libraries to occupy ~2% of total reads. Four samples were sequenced in one P3 lane on a NextSeq 2000 (NextSeq 2000 P3 reagents [100 cycles] 20040559).

CUT&RUN

CUT&RUN (Skene and Henikoff 2017) was performed with the following modifications. For FACS purification, >100,000 c-KIT$^+$ spermatogonia were attached to poly-D-lysine-coated (R&D Systems 3439-200-01) 24-well plates by centrifugation at 80*g* for 1 min (instead of binding to Concanavalin A beads). For low-input CUT&RUN, >20,000 THY1$^+$- and ITGa6$^+$- or c-KIT$^+$-sorted cells were used. After the attachment, cells were fixed with 1% formaldehyde in PBS for 15 min. After two PBS washes and one PBST wash (0.05% [v/v] Triton X-100), cells were incubated with primary antibodies in PBST BSA (0.05% Triton X-100, 3% BSA) overnight at 4°C. The next day, cells were washed twice with PBST and finally washed with 2 mM PBST EDTA. Cells were then incubated with 500 ng/mL pA-MNase (protein A-MNase) in PBST BSA EDTA for >1 h at 4°C. After pA-MNase binding, cells were washed twice with PBST EDTA, and the plate was placed on wet ice. Cells were then incubated in 200 µL of prechilled PBST with 2 mM $CaCl_2$ for 30 min. After MNase cutting, 200 µL of stop solution (340 mM NaCl, 20 mM EDTA, 4 mM EGTA, 50 µg/µL RNase A) was added, and the plate was placed for 15 min in a 37°C oven. Released cut fragments were decross-linked in 0.1% SDS and 125 µg/mL proteinase K (Sigma-Aldrich 03115828001) for >12 h in a 65°C oven. DNA was phenol-chloroform-extracted and sodium acetate/ethanol-precipitated. Resuspended DNA was further cleaned using 2.0× solid phase reversible immobilization (SPRI) beads to remove residual salts. Illumina sequencing libraries were generated based on a published protocol (Bowman et al. 2013) with the following modifications. SPRI beads were used in 2.0× ratio following end repair and A-tailings steps instead of 1.8×. Adapters were used at 2 nM final concentration instead of 10 nM. PCR extension was done for 30 sec instead of 45 sec. Between 12 and 17 cycles of library amplification indexing PCR were performed. The number of PCR cycles was determined in the exponential phase by a prerun of 10% of reaction with SYBR Green dye in a real-time PCR machine.

For low-input CUT&RUN, DNA was extracted using QIAquick PCR purification kit (Qiagen 28104) after releasing cut fragments. Illumina sequencing libraries were generated using NEBNext Ultra II DNA library preparation kit for Illumina kit (New England Biolabs E7645) based on the manufacturer's instructions. Adapters were used at 0.6 µM working concentration. Eleven cycles of library amplification indexing PCR were performed.

Computational analyses

Bulk RNA-seq For *Cbx2*^{KO} experiments, low-quality reads (Phred score 20) and adapter-containing reads (stringency 1) were trimmed using trim_galore (version 0.4.3) (Martin 2011). Trimmed reads were mapped to the mouse genome (mm10) with default parameters using STAR (version 2.5.3) (Dobin et al. 2013). Mapped reads were filtered with quality score 10 (-q 10), and only properly paired reads were retained (-f 2) using SAMtools (version 1.4.1) (Li et al. 2009). Counts per gene were obtained using featureCounts function of the subread package (version 1.5.0) (Liao et al. 2014). Using the count table, differentially expressed genes of c-KIT$^+$ spermatogonia between two *Cbx2*^{WT} and two *Cbx2*^{KO} animals were identified using the R (version 4.1.0) package edgeR (version 3.34.0) (Robinson et al. 2010). Because gene misexpression can be subtle and stochastic by mutations in cPRC1 components, a nonstringent cutoff of log fold change 0.2 and uncorrected *P*-value of 0.05 were used to obtain a sufficient number of genes to analyze their characteristics as a group. Data from *Cbx2*^{23KRA} experiments were processed identically to those of the *Cbx2*^{KO} experiment, except counts per gene were obtained with the strand parameter "-s 2" of featureCounts to account for the stranded library.

Analysis of standard single-cell RNA-seq For adult testis (Fig. 1), Cellranger count (Cellranger/2.0.0) was used to map FastQ files to the mouse genome (refdata-cellranger = mm10-1.2.0). We processed 141 million reads to obtain 875 cells with 162,000 mean reads and 2593 median number of detected genes per cell. Ten principal components were used for t-SNE visualization and k-means clustering. Data were visualized by the Loupe browser (10X Genomics).

For P15 testis (Fig. 2), P15 single-cell RNA-seq data were obtained from ArrayExpress (E-MTAB-6946, P15: do18195) (Ernst

et al. 2019). Cellranger count (cellranger/3.0.2) was used to map FastQ files to the mouse genome (refdata-cellranger-mm10-3.0.0) and obtain mtx files with UMI number-filtered raw expression values in each cell.

R package Seurat (R 3.6.3, Seurat 3.1.4) was used for all subsequent analyses (Stuart et al. 2019). Cells with >1000 detected RNA were used (nFeature_RNA > 1000) as done previously (Ernst et al. 2019). Ten principal components were used for clustering. From the initial clusters, spermatogonia and early spermatocytes were identified and chosen as a subset (3830 cells). The subset was reclustered with 10 principal components and resolution 0.25. Expression levels of groups of genes per cell were obtained by AddModuleScore function. Default parameters were used for all of the above analyses unless otherwise specified.

Analysis of amplicon single-cell RNA-seq of Cbx2-inducible KO Cellranger count (cellranger/6.0) was used to map FastQ files to the mouse genome (refdata-cellranger-mm10-3.0.0) and to obtain gene expression counts per cell. R package Seurat (R 4.1.0, Seurat 4.0.4) was used for subsequent analyses (Hao et al. 2021). Cells were filtered by (1) nFeature_RNA >2000, (2) mitochondrial RNA percentage <7.5, (3) percent occupied by the largest gene <3, and (4) RNA count and feature ratio <5.5 (see scripts posted on Github). Four control and four inducible KO samples were integrated to align cell populations across all four samples. Two control samples each generated from different mouse litters and batches of reagents were used as initial references for integration. Integrated data were then scaled and processed with 20 principal components for clustering. Differential gene expression tests were performed by the FindMarkers function of Seurat using Wilcoxon rank sum test.

Cbx2 genotypes were assigned based on independent *Cbx2* amplicon sequencing data using a custom Python script. The script identified "TGGCGCATCTGGTTCCTTGAGCTTGGAGCG" (WT, exon5 [underlined] linked to exon4) or "TGGCGCATCTGGTTCTTGGAGGACCAGCCG" (Mut, exon5 [underlined] linked to exon2) from the read2 of the paired-end reads and assigned the genotypes to the associated read1 (UMI-barcode). When an UMI was assigned to two different genotypes, likely due to PCR chimera formation, the genotype was left unassigned unless reads supporting one genotype were present 10 times more than the other genotype. A cell was assigned to be "Mut" when all *Cbx2* amplicon reads showed recombination (exon5 linked to exon2) and otherwise was assigned to be "WT or Het." Only the cells that had at least four UMIs linked to *Cbx2* sequence were assigned genotypes. The metadata for their genotypes (WT/Het or Mut) were added to the Seurat object by the AddMetaData function.

Analysis of CUT&RUN data Paired-end FastQ reads were quality-trimmed (score 20) with stringency 1 using trim_galore (version 0.4.3) (Martin 2011). Trimmed reads were mapped to the mm10 genome using bowtie2 (version 2.3.1) with the end-to-end option (Langmead and Salzberg 2012). Mapped reads were quality-filtered with MAPQ >10, and only properly paired reads were retained using SAMtools (version 1.4.1) (Li et al. 2009). Picard (version 2.17.1; http://broadinstitute.github.io/picard) was used to remove duplicate reads. Alignment files (bam) were converted to bigwig files using Deeptools (version 2.2.4) by normalizing with RPKM (Ramírez et al. 2016). Peaks were identified by using MACS2 (version 2.1) with the "--broad" option by comparing CUT&RUN results using CBX2 antibodies (experimental) with IgG (control) or using HA antibodies applied to $Cbx2^{HA/HA}$ (experimental) or $Cbx2^{+/+}$ (control) mice (Zhang et al. 2008). CBX2 target genes were selected by first choosing the genes with transcription start sites overlapping with the CBX2 peaks and only retaining the ones with more than one CBX2 (antibodies 855 and 856) or CBX2-HA (antibodies 16B12 and ab9110) CUT&RUN result showing that the gene is a target. Enrichment heat maps and numeric data for averaged plots were obtained using the computeMatrix tool from Deeptools. Averaged plots were drawn by Matlab. Promoter-associated enrichment scores were obtained using the multiBigwigSummary function of Deeptools. For a comparative visualization of CUT&RUN experiments in two different cell types (e.g., wild type vs. 23KRA), signal intensities for the same antibody were TMM-normalized with values from all 27,848 promoters ±5 kb centered at TSSs using EdgeR's calcNormFactors function.

Data availability

The data sets and computer code produced in this study are available in the following databases: Single-cell RNA-seq data are available at Gene Expression Omnibus under accession number GSE210368 (https://www.ncbi.nlm.nih.gov/geo/query/acc.cgi?acc=GSE210368). Bulk RNA-seq data are available at Gene Expression Omnibus under accession number GSE222146 (https://www.ncbi.nlm.nih.gov/geo/query/acc.cgi?acc=GSE222146). CUT&RUN data are available at Gene Expression Omnibus under accession number GSE210367 (https://www.ncbi.nlm.nih.gov/geo/query/acc.cgi?acc=GSE210367). All analysis scripts are available at https://github.com/jongminkmg/Cbx2.

Competing interest statement

The authors declare no competing interests.

Acknowledgments

We thank Minx Fuller and members of the Fuller, Page, and Kingston laboratory for insightful discussions. We thank Tsutomu Endo for advice on mammalian spermatogenesis, Lin Wu (Harvard Genome Modification Facility) for *HA-Cbx2* knock-in mouse generation, Manashree Damle for advice on bioinformatic analyses, and the Jen Sheen, Susan Cotman, and Jeannie Lee laboratories for help and access to microscopes. We thank MacKenzie Mauger, Wojciech Siwek, Ukrae Cho, Julia Wucherpfennig, Theresa Oei, and Hun-Goo Lee for careful reading of the manuscript. J.J.K. was supported by the Urology Care Foundation Research Scholar Award Program (2018A012748), M.S.L. was supported by the Agency of Science, Research, and Technology, Singapore, and D.C.P. was supported by Howard Hughes Medical Institute. This work was supported by National Institutes of Health grants R01GM4390121A1 and R35GM131743 to R.E.K. The content is the responsibility of the authors and does not represent the views of the funders.

Author contributions: J.J.K. and R.E.K conceived the study. J.J.K. and E.R.S. performed experiments and data analysis. M.S.L. generated $Cbx2^{\Delta}$ mice. D.G.R. and D.C.P. advised on characterization of *Cbx2* mutant testis phenotypes. J.J.K. and R.E.K. wrote the manuscript with input from all authors.

References

Ahmed EA, de Rooij DG. 2009. Staging of mouse seminiferous tubule cross-sections. *Methods Mol Biol* **558:** 263–277. doi:10.1007/978-1-60761-103-5_16

Aloisio GM, Nakada Y, Saatcioglu HD, Peña CG, Baker MD, Tarnawa ED, Mukherjee J, Manjunath H, Bugde A, Sengupta AL, et al. 2014. PAX7 expression defines germline stem cells in the

adult testis. *J Clin Invest* **124:** 3929–3944. doi:10.1172/JCI75943

Bantignies F, Roure V, Comet I, Leblanc B, Schuettengruber B, Bonnet J, Tixier V, Mas A, Cavalli G. 2011. Polycomb-dependent regulatory contacts between distant Hox loci in *Drosophila*. *Cell* **144:** 214–226. doi:10.1016/j.cell.2010.12.026

Beh LY, Colwell LJ, Francis NJ. 2012. A core subunit of Polycomb repressive complex 1 is broadly conserved in function but not primary sequence. *Proc Natl Acad Sci* **109:** E1063–E1071.

Beliveau BJ, Joyce EF, Apostolopoulos N, Yilmaz F, Fonseka CY, McCole RB, Chang Y, Li JB, Senaratne TN, Williams BR, et al. 2012. Versatile design and synthesis platform for visualizing genomes with Oligopaint FISH probes. *Proc Natl Acad Sci* **109:** 21301–21306. doi:10.1073/pnas.1213818110

Beumer TL, Roepers-Gajadien HL, Gademan IS, Kal HB, de Rooij DG. 2000. Involvement of the D-type cyclins in germ cell proliferation and differentiation in the mouse. *Biol Reprod* **63:** 1893–1898. doi:10.1095/biolreprod63.6.1893

Blackledge NP, Klose RJ. 2021. The molecular principles of gene regulation by Polycomb repressive complexes. *Nat Rev Mol Cell Biol* **22:** 815–833. doi:10.1038/s41580-021-00398-y

Bowman SK, Simon MD, Deaton AM, Tolstorukov M, Borowsky ML, Kingston RE. 2013. Multiplexed illumina sequencing libraries from picogram quantities of DNA. *BMC Genomics* **14:** 466. doi:10.1186/1471-2164-14-466

Buaas FW, Kirsh AL, Sharma M, McLean DJ, Morris JL, Griswold MD, de Rooij DG, Braun RE. 2004. Plzf is required in adult male germ cells for stem cell self-renewal. *Nat Genet* **36:** 647–652. doi:10.1038/ng1366

Cao R, Wang L, Wang H, Xia L, Erdjument-Bromage H, Tempst P, Jones RS, Zhang Y. 2002. Role of histone H3 lysine 27 methylation in Polycomb-group silencing. *Science* **298:** 1039–1043. doi:10.1126/science.1076997

Chamberlain SJ, Yee D, Magnuson T. 2008. Polycomb repressive complex 2 is dispensable for maintenance of embryonic stem cell pluripotency. *Stem Cells* **26:** 1496–1505. doi:10.1634/stemcells.2008-0102

Chiacchiera F, Rossi A, Jammula S, Piunti A, Scelfo A, Ordóñez-Morán P, Huelsken J, Koseki H, Pasini D. 2016. Polycomb complex PRC1 preserves intestinal stem cell identity by sustaining Wnt/β-catenin transcriptional activity. *Cell Stem Cell* **18:** 91–103. doi:10.1016/j.stem.2015.09.019

Core N, Bel S, Gaunt SJ, Aurrand-Lions M, Pearce J, Fisher A, Djabali M. 1997. Altered cellular proliferation and mesoderm patterning in Polycomb-M33-deficient mice. *Development* **124:** 721–729. doi:10.1242/dev.124.3.721

Costoya JA, Hobbs RM, Barna M, Cattoretti G, Manova K, Sukhwani M, Orwig KE, Wolgemuth DJ, Pandolfi PP. 2004. Essential role of Plzf in maintenance of spermatogonial stem cells. *Nat Genet* **36:** 653–659. doi:10.1038/ng1367

Czermin B, Melfi R, McCabe D, Seitz V, Imhof A, Pirrotta V. 2002. *Drosophila* enhancer of Zeste/ESC complexes have a histone H3 methyltransferase activity that marks chromosomal Polycomb sites. *Cell* **111:** 185–196. doi:10.1016/S0092-8674(02)00975-3

Dauber KL, Perdigoto CN, Valdes VJ, Santoriello FJ, Cohen I, Ezhkova E. 2016. Dissecting the roles of Polycomb repressive complex 2 subunits in the control of skin development. *J Invest Dermatol* **136:** 1647–1655. doi:10.1016/j.jid.2016.02.809

de Rooij DG, Russell LD. 2000. All you wanted to know about spermatogonia but were afraid to ask. *J Androl* **21:** 776–798.

de Rooij DG, Lok D, Weenk D. 1985. Feedback regulation of the proliferation of the undifferentiated spermatogonia in the Chinese hamster by the differentiating spermatogonia. *Cell Tissue Kinet* **18:** 71–81.

Dobin A, Davis CA, Schlesinger F, Drenkow J, Zaleski C, Jha S, Batut P, Chaisson M, Gingeras TR. 2013. STAR: ultrafast universal RNA-seq aligner. *Bioinformatics* **29:** 15–21. doi:10.1093/bioinformatics/bts635

Endo T, Romer KA, Anderson EL, Baltus AE, de Rooij DG, Page DC. 2015. Periodic retinoic acid–STRA8 signaling intersects with periodic germ-cell competencies to regulate spermatogenesis. *Proc Natl Acad Sci* **112:** E2347–E2356. doi:10.1073/pnas.1505683112

Ernst C, Eling N, Martinez-Jimenez CP, Marioni JC, Odom DT. 2019. Staged developmental mapping and X chromosome transcriptional dynamics during mouse spermatogenesis. *Nat Commun* **10:** 1251. doi:10.1038/s41467-019-09182-1

Flora P, Dalal G, Cohen I, Ezhkova E. 2021. Polycomb repressive complex(es) and their role in adult stem cells. *Genes (Basel)* **12:** 1485. doi:10.3390/genes12101485

Francis NJ, Kingston RE, Woodcock CL. 2004. Chromatin compaction by a polycomb group protein complex. *Science* **306:** 1574–1577. doi:10.1126/science.1100576

Gao Z, Zhang J, Bonasio R, Strino F, Sawai A, Parisi F, Kluger Y, Reinberg D. 2012. PCGF homologs, CBX proteins, and RYBP define functionally distinct PRC1 family complexes. *Mol Cell* **45:** 344–356. doi:10.1016/j.molcel.2012.01.002

Garcia-Moreno SA, Lin YT, Futtner CR, Salamone IM, Capel B, Maatouk DM. 2019. CBX2 is required to stabilize the testis pathway by repressing Wnt signaling. *PLoS Genet* **15:** e1007895. doi:10.1371/journal.pgen.1007895

Gely-Pernot A, Raverdeau M, Célébi C, Dennefeld C, Feret B, Klopfenstein M, Yoshida S, Ghyselinck NB, Mark M. 2012. Spermatogonia differentiation requires retinoic acid receptor γ. *Endocrinology* **153:** 438–449. doi:10.1210/en.2011-1102

Grau DJ, Chapman BA, Garlick JD, Borowsky M, Francis NJ, Kingston RE. 2011. Compaction of chromatin by diverse Polycomb group proteins requires localized regions of high charge. *Genes Dev* **25:** 2210–2221. doi:10.1101/gad.17288211

Grimaud C, Bantignies F, Pal-Bhadra M, Ghana P, Bhadra U, Cavalli G. 2006. RNAi components are required for nuclear clustering of Polycomb group response elements. *Cell* **124:** 957–971. doi:10.1016/j.cell.2006.01.036

Hao Y, Hao S, Andersen-Nissen E, Mauck WM III, Zheng S, Butler A, Lee MJ, Wilk AJ, Darby C, Zager M, et al. 2021. Integrated analysis of multimodal single-cell data. *Cell* **184:** 3573–3587.e29. doi:10.1016/j.cell.2021.04.048

Hasegawa K, Sin HS, Maezawa S, Broering TJ, Kartashov AV, Alavattam KG, Ichijima Y, Zhang F, Bacon WC, Greis KD, et al. 2015. SCML2 establishes the male germline epigenome through regulation of histone H2A ubiquitination. *Dev Cell* **32:** 574–588. doi:10.1016/j.devcel.2015.01.014

Hofmann MC, Braydich-Stolle L, Dym M. 2005. Isolation of male germ-line stem cells; influence of GDNF. *Dev Biol* **279:** 114–124. doi:10.1016/j.ydbio.2004.12.006

Ikami K, Tokue M, Sugimoto R, Noda C, Kobayashi S, Hara K, Yoshida S. 2015. Hierarchical differentiation competence in response to retinoic acid ensures stem cell maintenance during mouse spermatogenesis. *Development* **142:** 1582–1592.

Isono K, Endo TA, Ku M, Yamada D, Suzuki R, Sharif J, Ishikura T, Toyoda T, Bernstein BE, Koseki H. 2013. SAM domain polymerization links subnuclear clustering of PRC1 to gene silencing. *Dev Cell* **26:** 565–577. doi:10.1016/j.devcel.2013.08.016

Jaensch ES, Zhu J, Cochrane JC, Marr SK, Oei TA, Damle M, McCaslin EZ, Kingston RE. 2021. A Polycomb domain found in committed cells impairs differentiation when introduced into PRC1 in pluripotent cells. *Mol Cell* **81:** 4677–4691.e8. doi:10.1016/j.molcel.2021.09.018

Katoh-Fukui Y, Tsuchiya R, Shiroishi T, Nakahara Y, Hashimoto N, Noguchi K, Higashinakagawa T. 1998. Male-to-female sex reversal in M33 mutant mice. *Nature* **393:** 688–692. doi:10.1038/31482

Katoh-Fukui Y, Owaki A, Toyama Y, Kusaka M, Shinohara Y, Maekawa M, Toshimori K, Morohashi K. 2005. Mouse Polycomb M33 is required for splenic vascular and adrenal gland formation through regulating Ad4BP/SF1 expression. *Blood* **106:** 1612–1620. doi:10.1182/blood-2004-08-3367

Katoh-Fukui Y, Baba T, Sato T, Otake H, Nagakui-Noguchi Y, Shindo M, Suyama M, Ohkawa Y, Tsumura H, Morohashi KI, et al. 2019. Mouse polycomb group gene Cbx2 promotes osteoblastic but suppresses adipogenic differentiation in postnatal long bones. *Bone* **120:** 219–231. doi:10.1016/j.bone.2018.10.021

Kim JJ, Kingston RE. 2022. Context-specific Polycomb mechanisms in development. *Nat Rev Genet* **23:** 680–695. doi:10.1038/s41576-022-00499-0

Kishi JY, Lapan SW, Beliveau BJ, West ER, Zhu A, Sasaki HM, Saka SK, Wang Y, Cepko CL, Yin P. 2019. SABER amplifies FISH: enhanced multiplexed imaging of RNA and DNA in cells and tissues. *Nat Methods* **16:** 533–544. doi:10.1038/s41592-019-0404-0

Komai Y, Tanaka T, Tokuyama Y, Yanai H, Ohe S, Omachi T, Atsumi N, Yoshida N, Kumano K, Hisha H, et al. 2014. Bmi1 expression in long-term germ stem cells. *Sci Rep* **4:** 6175. doi:10.1038/srep06175

Kondo T, Isono K, Kondo K, Endo TA, Itohara S, Vidal M, Koseki H. 2014. Polycomb potentiates meis2 activation in midbrain by mediating interaction of the promoter with a tissue-specific enhancer. *Dev Cell* **28:** 94–101. doi:10.1016/j.devcel.2013.11.021

Koppens MA, Bounova G, Gargiulo G, Tanger E, Janssen H, Cornelissen-Steijger P, Blom M, Song JY, Wessels LF, van Lohuizen M. 2016. Deletion of Polycomb repressive complex 2 from mouse intestine causes loss of stem cells. *Gastroenterology* **151:** 684–697.e12. doi:10.1053/j.gastro.2016.06.020

Kotaja N, Kimmins S, Brancorsini S, Hentsch D, Vonesch JL, Davidson I, Parvinen M, Sassone-Corsi P. 2004. Preparation, isolation and characterization of stage-specific spermatogenic cells for cellular and molecular analysis. *Nat Methods* **1:** 249–254. doi:10.1038/nmeth1204-249

Koubova J, Menke DB, Zhou Q, Capel B, Griswold MD, Page DC. 2006. Retinoic acid regulates sex-specific timing of meiotic initiation in mice. *Proc Natl Acad Sci* **103:** 2474–2479. doi:10.1073/pnas.0510813103

Kundu S, Ji F, Sunwoo H, Jain G, Lee JT, Sadreyev RI, Dekker J, Kingston RE. 2017. Polycomb repressive complex 1 generates discrete compacted domains that change during differentiation. *Mol Cell* **65:** 432–446.e5. doi:10.1016/j.molcel.2017.01.009

Kuzmichev A, Nishioka K, Erdjument-Bromage H, Tempst P, Reinberg D. 2002. Histone methyltransferase activity associated with a human multiprotein complex containing the enhancer of Zeste protein. *Genes Dev* **16:** 2893–2905. doi:10.1101/gad.1035902

Langmead B, Salzberg SL. 2012. Fast gapped-read alignment with Bowtie 2. *Nat Methods* **9:** 357–359. doi:10.1038/nmeth.1923

Larson AG, Elnatan D, Keenen MM, Trnka MJ, Johnston JB, Burlingame AL, Agard DA, Redding S, Narlikar GJ. 2017. Liquid droplet formation by HP1α suggests a role for phase separation in heterochromatin. *Nature* **547:** 236–240. doi:10.1038/nature22822

Lau MS. 2016. "Mutations in the charged domain of CBX2 disrupt PRC1 function in vivo." PhD thesis, Medical Sciences Harvard University, Cambridge, MA.

Lau MS, Schwartz MG, Kundu S, Savol AJ, Wang PI, Marr SK, Grau DJ, Schorderet P, Sadreyev RI, Tabin CJ, et al. 2017. Mutation of a nucleosome compaction region disrupts Polycomb-mediated axial patterning. *Science* **355:** 1081–1084. doi:10.1126/science.aah5403

Lee S, Abini-Agbomson S, Perry DS, Goodman A, Rao B, Huang MY, Diedrich JK, Moresco JJ, Yates JR III, Armache KJ, et al. 2023. Intrinsic mesoscale properties of a Polycomb protein underpin heterochromatin fidelity. *Nat Struct Mol Biol* **30:** 891–901. doi: 10.1038/s41594-023-01000-z

Lessard J, Sauvageau G. 2003. Bmi-1 determines the proliferative capacity of normal and leukaemic stem cells. *Nature* **423:** 255–260. doi:10.1038/nature01572

Lessard J, Baban S, Sauvageau G. 1998. Stage-specific expression of polycomb group genes in human bone marrow cells. *Blood* **91:** 1216–1224. doi:10.1182/blood.V91.4.1216

Levine SS, Weiss A, Erdjument-Bromage H, Shao Z, Tempst P, Kingston RE. 2002. The core of the polycomb repressive complex is compositionally and functionally conserved in flies and humans. *Mol Cell Biol* **22:** 6070–6078. doi:10.1128/MCB.22.17.6070-6078.2002

Li L, Clevers H. 2010. Coexistence of quiescent and active adult stem cells in mammals. *Science* **327:** 542–545. doi:10.1126/science.1180794

Li H, Handsaker B, Wysoker A, Fennell T, Ruan J, Homer N, Marth G, Abecasis G, Durbin R Genome Project Data Processing S. 2009. The sequence alignment/map format and SAMtools. *Bioinformatics* **25:** 2078–2079. doi:10.1093/bioinformatics/btp352

Liao Y, Smyth GK, Shi W. 2014. featureCounts: an efficient general purpose program for assigning sequence reads to genomic features. *Bioinformatics* **30:** 923–930. doi:10.1093/bioinformatics/btt656

Lovasco LA, Gustafson EA, Seymour KA, de Rooij DG, Freiman RN. 2015. TAF4b is required for mouse spermatogonial stem cell development. *Stem Cells* **33:** 1267–1276. doi:10.1002/stem.1914

Maezawa S, Hasegawa K, Yukawa M, Sakashita A, Alavattam KG, Andreassen PR, Vidal M, Koseki H, Barski A, Namekawa SH. 2017. Polycomb directs timely activation of germline genes in spermatogenesis. *Genes Dev* **31:** 1693–1703. doi:10.1101/gad.302000.117

Maezawa S, Hasegawa K, Yukawa M, Kubo N, Sakashita A, Alavattam KG, Sin HS, Kartashov AV, Sasaki H, Barski A, et al. 2018. Polycomb protein SCML2 facilitates H3K27me3 to establish bivalent domains in the male germline. *Proc Natl Acad Sci* **115:** 4957–4962. doi:10.1073/pnas.1804512115

Martin M. 2011. CutAdapt removes adapter sequences from high-throughput sequencing reads. *EMBnetj* **17:** 10–12. doi:10.14806/ej.17.1.200

Molofsky AV, Pardal R, Iwashita T, Park IK, Clarke MF, Morrison SJ. 2003. Bmi-1 dependence distinguishes neural stem cell self-renewal from progenitor proliferation. *Nature* **425:** 962–967. doi:10.1038/nature02060

Morey L, Pascual G, Cozzuto L, Roma G, Wutz A, Benitah SA, Di Croce L. 2012. Nonoverlapping functions of the Polycomb group Cbx family of proteins in embryonic stem cells. *Cell Stem Cell* **10:** 47–62. doi:10.1016/j.stem.2011.12.006

Mu W, Starmer J, Fedoriw AM, Yee D, Magnuson T. 2014. Repression of the soma-specific transcriptome by Polycomb-repressive complex 2 promotes male germ cell development. *Genes Dev* **28:** 2056–2069. doi:10.1101/gad.246124.114

Müller J, Hart CM, Francis NJ, Vargas ML, Sengupta A, Wild B, Miller EL, O'Connor MB, Kingston RE, Simon JA. 2002. Histone methyltransferase activity of a *Drosophila* Polycomb group repressor complex. *Cell* **111:** 197–208. doi:10.1016/S0092-8674(02)00976-5

Nam AS, Kim KT, Chaligne R, Izzo F, Ang C, Taylor J, Myers RM, Abu-Zeinah G, Brand R, Omans ND, et al. 2019. Somatic mutations and cell identity linked by genotyping of transcriptomes. *Nature* **571:** 355–360. doi:10.1038/s41586-019-1367-0

O'Loghlen A, Munoz-Cabello AM, Gaspar-Maia A, Wu HA, Banito A, Kunowska N, Racek T, Pemberton HN, Beolchi P, Lavial F, et al. 2012. MicroRNA regulation of Cbx7 mediates a switch of Polycomb orthologs during ESC differentiation. *Cell Stem Cell* **10:** 33–46. doi:10.1016/j.stem.2011.12.004

Park IK, Qian D, Kiel M, Becker MW, Pihalja M, Weissman IL, Morrison SJ, Clarke MF. 2003. Bmi-1 is required for maintenance of adult self-renewing haematopoietic stem cells. *Nature* **423:** 302–305. doi:10.1038/nature01587

Parreno V, Martinez AM, Cavalli G. 2022. Mechanisms of Polycomb group protein function in cancer. *Cell Res* **32:** 231–253. doi:10.1038/s41422-021-00606-6

Piunti A, Rossi A, Cerutti A, Albert M, Jammula S, Scelfo A, Cedrone L, Fragola G, Olsson L, Koseki H, et al. 2014. Polycomb proteins control proliferation and transformation independently of cell cycle checkpoints by regulating DNA replication. *Nat Commun* **5:** 3649. doi:10.1038/ncomms4649

Plys AJ, Davis CP, Kim J, Rizki G, Keenen MM, Marr SK, Kingston RE. 2019. Phase separation of Polycomb-repressive complex 1 is governed by a charged disordered region of CBX2. *Genes Dev* **33:** 799–813. doi:10.1101/gad.326488.119

Ramírez F, Ryan DP, Grüning B, Bhardwaj V, Kilpert F, Richter AS, Heyne S, Dündar F, Manke T. 2016. deepTools2: a next generation web server for deep-sequencing data analysis. *Nucleic Acids Res* **44:** W160–W165. doi:10.1093/nar/gkw257

Robinson MD, McCarthy DJ, Smyth GK. 2010. edgeR: a Bioconductor package for differential expression analysis of digital gene expression data. *Bioinformatics* **26:** 139–140. doi:10.1093/bioinformatics/btp616

Satijn DP, Gunster MJ, van der Vlag J, Hamer KM, Schul W, Alkema MJ, Saurin AJ, Freemont PS, van Driel R, Otte AP. 1997. RING1 is associated with the polycomb group protein complex and acts as a transcriptional repressor. *Mol Cell Biol* **17:** 4105–4113. doi:10.1128/MCB.17.7.4105

Saurin AJ, Shiels C, Williamson J, Satijn DP, Otte AP, Sheer D, Freemont PS. 1998. The human polycomb group complex associates with pericentromeric heterochromatin to form a novel nuclear domain. *J Cell Biol* **142:** 887–898. doi:10.1083/jcb.142.4.887

Schindelin J, Arganda-Carreras I, Frise E, Kaynig V, Longair M, Pietzsch T, Preibisch S, Rueden C, Saalfeld S, Schmid B, et al. 2012. Fiji: an open-source platform for biological-image analysis. *Nat Methods* **9:** 676–682. doi:10.1038/nmeth.2019

Schmidt JA, Oatley JM, Brinster RL. 2009. Female mice delay reproductive aging in males. *Biol Reprod* **80:** 1009–1014. doi:10.1095/biolreprod.108.073619

Seif E, Kang JJ, Sasseville C, Senkovich O, Kaltashov A, Boulier EL, Kapur I, Kim CA, Francis NJ. 2020. Phase separation by the polyhomeotic sterile α motif compartmentalizes Polycomb group proteins and enhances their activity. *Nat Commun* **11:** 5609. doi:10.1038/s41467-020-19435-z

Shao Z, Raible F, Mollaaghababa R, Guyon JR, Wu CT, Bender W, Kingston RE. 1999. Stabilization of chromatin structure by PRC1, a Polycomb complex. *Cell* **98:** 37–46. doi:10.1016/S0092-8674(00)80604-2

Shinohara T, Orwig KE, Avarbock MR, Brinster RL. 2000. Spermatogonial stem cell enrichment by multiparameter selection of mouse testis cells. *Proc Natl Acad Sci* **97:** 8346–8351. doi:10.1073/pnas.97.15.8346

Skarnes WC, Rosen B, West AP, Koutsourakis M, Bushell W, Iyer V, Mujica AO, Thomas M, Harrow J, Cox T, et al. 2011. A conditional knockout resource for the genome-wide study of mouse gene function. *Nature* **474:** 337–342. doi:10.1038/nature10163

Skene PJ, Henikoff S. 2017. An efficient targeted nuclease strategy for high-resolution mapping of DNA binding sites. *Elife* **6:** e21856. doi:10.7554/eLife.21856

Strom AR, Emelyanov AV, Mir M, Fyodorov DV, Darzacq X, Karpen GH. 2017. Phase separation drives heterochromatin domain formation. *Nature* **547:** 241–245. doi:10.1038/nature22989

Stuart T, Butler A, Hoffman P, Hafemeister C, Papalexi E, Mauck WM III, Hao Y, Stoeckius M, Smibert P, Satija R. 2019. Comprehensive integration of single-cell data. *Cell* **177:** 1888–1902 e1821. doi:10.1016/j.cell.2019.05.031

Takada Y, Isono K, Shinga J, Turner JM, Kitamura H, Ohara O, Watanabe G, Singh PB, Kamijo T, Jenuwein T, et al. 2007. Mammalian Polycomb Scmh1 mediates exclusion of Polycomb complexes from the XY body in the pachytene spermatocytes. *Development* **134:** 579–590. doi:10.1242/dev.02747

Tatavosian R, Kent S, Brown K, Yao T, Duc HN, Huynh TN, Zhen CY, Ma B, Wang H, Ren X. 2019. Nuclear condensates of the Polycomb protein chromobox 2 (CBX2) assemble through phase separation. *J Biol Chem* **294:** 1451–1463. doi:10.1074/jbc.RA118.006620

Tsumura A, Hayakawa T, Kumaki Y, Takebayashi S, Sakaue M, Matsuoka C, Shimotohno K, Ishikawa F, Li E, Ueda HR, et al. 2006. Maintenance of self-renewal ability of mouse embryonic stem cells in the absence of DNA methyltransferases Dnmt1, Dnmt3a and Dnmt3b. *Genes Cells* **11:** 805–814. doi:10.1111/j.1365-2443.2006.00984.x

Wei C, Lin H, Cui S. 2018. The forkhead transcription factor FOXC2 is required for maintaining murine spermatogonial stem cells. *Stem Cells Dev* **27:** 624–636. doi:10.1089/scd.2017.0233

Xie H, Xu J, Hsu JH, Nguyen M, Fujiwara Y, Peng C, Orkin SH. 2014. Polycomb repressive complex 2 regulates normal hematopoietic stem cell function in a developmental-stage-specific manner. *Cell Stem Cell* **14:** 68–80. doi:10.1016/j.stem.2013.10.001

Yoshida S, Sukeno M, Nabeshima Y. 2007. A vasculature-associated niche for undifferentiated spermatogonia in the mouse testis. *Science* **317:** 1722–1726. doi:10.1126/science.1144885

Zhang Y, Liu T, Meyer CA, Eeckhoute J, Johnson DS, Bernstein BE, Nusbaum C, Myers RM, Brown M, Li W, et al. 2008. Model-based analysis of ChIP-seq (MACS). *Genome Biol* **9:** R137. doi:10.1186/gb-2008-9-9-r137

Zhen CY, Tatavosian R, Huynh TN, Duc HN, Das R, Kokotovic M, Grimm JB, Lavis LD, Lee J, Mejia FJ, et al. 2016. Live-cell single-molecule tracking reveals co-recognition of H3K27me3 and DNA targets polycomb Cbx7-PRC1 to chromatin. *Elife* **5:** e17667. doi:10.7554/eLife.17667

Zhou Q, Li Y, Nie R, Friel P, Mitchell D, Evanoff RM, Pouchnik D, Banasik B, McCarrey JR, Small C, et al. 2008. Expression of stimulated by retinoic acid gene 8 (Stra8) and maturation of murine gonocytes and spermatogonia induced by retinoic acid in vitro. *Biol Reprod* **78:** 537–545. doi:10.1095/biolreprod.107.064337

Cell type-specific role of CBX2 and its disordered region in spermatogenesis

Jongmin J. Kim, Emma R. Steinson, Mei Sheng Lau, et al.

Genes Dev. published online August 8, 2023
Access the most recent version at doi:10.1101/gad.350393.122